

**MAJOR PROJECT**  
**ON**  
**DESIGN AND ANALYSIS OF TIDAL TURBINE**

*Submitted by:*

**G. Mohith Sai** **221710801011**

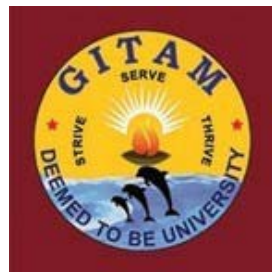
**B.V.D Naga Teja** **221710801046**

**Yathindra Abhinav.S** **221710801049**

*Under the Supervision of:*

**Mr. J. Ramesh**

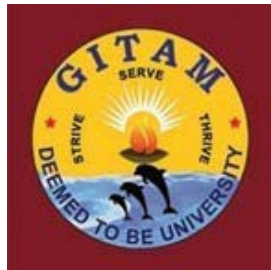
Asst. Professor



**DEPARTMENT OF MECHANICAL ENGINEERING**  
**GITAM SCHOOL OF TECHNOLOGY**  
**GITAM, HYDERABAD**

**May 2021**

**DEPARTMENT OF MECHANICAL ENGINEERING  
GITAM SCHOOL OF TECHNOLOGY  
GITAM, HYDERABAD**



**CERTIFICATE**

This is to certify that the thesis entitled "**DESIGN AND ANALYSIS OF TIDAL TURBINE**" submitted to GITAM University, Hyderabad by **G. Mohith Sai, B.V.D. Naga Teja, Yathindra Abhinav.S** for the award of **Major Project** in **Mechanical Engineering** is a record of bonafide research work carried out by them. The results embodied in this thesis have not been submitted to any other University or Institute for the award of any degree.

**Supervisor**

Mr. J. Ramesh  
Asst. Professor,  
GITAM School of Technology  
Hyderabad Campus.

**Head of the Department**

Dr. P. Eshwaraiah  
Professor  
Department of Mechanical Engineering  
GITAM School of Technology

**Project coordinator**

Mr. B. Bhasker  
Asst. Professor,  
GITAM School of Technology  
Hyderabad Campus.

## **DECLARATION**

I, hereby declare that the work entitled "**DESIGN AND ANALYSIS OF TIDAL TURBINE**" submitted to the department of Mechanical Engineering, GITAM University is a record of an original work carried out by me under the guidance of **J. Ramesh**. This report is submitted in partial fulfilment of requirement for the award of Major Project in **BACHELOR OF TECHNOLOGY in MECHANICAL ENGINEERING**. I declare that the work reported in this report has not been reported and will not be submitted to any university for the award of Degree.

### **Signature**

G. Mohith Sai 221710801011

B.V.D. Naga Teja 221710801046

Yathindra Abhinav.S 221710801049

## **ABSTRACT**

In the present world, there is massive energy demand. Most of this energy is supplied by using coal, crude oil, fossil fuels which is harmful to the environment and causes high carbon emissions and global warming. We need more alternative resources which are renewable. For renewable energy, we have many sources such as Wind Energy, Solar energy, Geothermal energy, Hydroelectric energy, and Tidal energy, etc. There are only a few tidal power plants located all over the world.

In tidal energy, the current velocity of water is taken by the blade, and it is converted to rotational energy. A series of generators couple this rotational energy to produce energy. More study is required for more power plants to harvest electricity from natural tides effectively, so more work should be put into harnessing tidal energy.

Before designing blade rated, power calculation of a turbine needs to be done for a turbine. Using Blade element and momentum theory (BEMT), a design is created to place the turbine at a depth of 120 m below sea level.

Boundary conditions like pressure and tidal current velocity are taken from the reference papers for CFD simulation. The outcomes of the CFD simulation are the velocity of fluid, pressure on blades, turbulent kinetic energy, eddy viscosity, turbulent eddy frequency, velocity vector, streamline thrust force acting on the blade and torque from the rotation of the blade for different tip speed ratios. This would give a better understanding of how efficient is the designed turbine for power extraction.

A Static Structural Analysis is done to check for stresses, forces, and strain due to the pressure acting at higher depth on the blade. Finally, a Modal analysis is done to check for frequencies, vibrations, and noises generated by the blade to avoid resonance.

## **ACKNOWLEDGMENT**

Apart from our effort, the success of this Major Project largely depends on the encouragement and guidance of many others. We take this opportunity to express our gratitude to the people who have helped us in the successful competition of this Major Project.

We would like to thank J. Ramesh Sir for great guidance and encouragement for doing this project and Burra Bhaskar Sir for making us improve our working skills in this major project.

We would like to thank respected Eshwaraiah P, Head of the Department of MECHANICAL Engineering, for giving us such an excellent opportunity to expand our knowledge for our own branch and giving us guidelines to present a Major Project report. It helped us a lot to realize what we study for.

We would like to thank the respected faculties who helped us to make this Major Project a successful accomplishment.

We would also like to thank our teammates, who helped us to make our work more organized and well-stacked till the end.

## CONTENTS

	Page No
Certificate.....	i
Declaration.....	ii
Abstract.....	iii
Acknowledgement.....	iv
List of Figures.....	vii
List of Tables.....	viii
Chapter-1 Introduction.....	1
1.1 Ocean Energy.....	1
1.1.1 Global Potential.....	1
1.2 Forms of Ocean Energy.....	2
1.3 Tide.....	2
1.3.1 Characteristics.....	2
1.3.2 Definitions.....	3
1.4 Methods to Extract Tidal Energy.....	4
1.4.1 Tidal Barrages.....	5
1.4.2 Tidal Stream Energy.....	5
Chapter-2 Literature Review.....	7
2.1 Literature Survey.....	7
2.2 Motivation for the Present Work.....	12
Chapter-3 Objectives and Methodology.....	13

3.1 Objectives.....	13
3.2 Methodology.....	13
3.2.1 Betz Limit Theory.....	13
3.2.2 Blade Element Momentum Theory.....	14
3.2.3 Static Structural Analysis.....	15
3.2.4 Cantilever Beam.....	16
3.2.5 Finite Element Analysis.....	16
3.2.6 Modal Analysis.....	16
3.2.7 Computational Fluid Dynamics.....	17
3.2.8 Finite Volume Method.....	17
3.2.9 Shear Stress Transport.....	18
Chapter-4 Numerical Analysis.....	19
4.1 Blade Element Momentum Analysis.....	19
4.2 Static Structural Analysis.....	20
4.3 Modal Analysis.....	21
4.4 Flow Analysis.....	22
Chapter-5 Results and Discussions.....	24
5.1 Static Structural Analysis Results.....	24
5.2 Modal Analysis Results.....	26
5.3 Flow Analysis Results.....	28
Chapter-6 Conclusions.....	47
References.....	48

## LIST OF FIGURES

1. Fig 1.1: Distribution of Tide Phases.....	3
2. Fig 1.2: Depiction of Various Tides.....	4
3. Fig 1.3: Tidal Barrage.....	5
4. Fig 1.4: Various Tidal Stream Devices.....	6
5. Fig 3.1: Blade Element Momentum Demonstration.....	14
6. Fig 3.2: Blade Element Momentum Method for Designing Blade.....	14
7. Fig 3.3: Blade as Cantilever Beam for Static Structural Analysis.....	16
8. Fig 3.4: Blade as Cantilever Beam for Modal Analysis.....	17
9. Fig 4.1: Setup for Static Structural Analysis.....	20
10. Fig 4.2: Mesh for Static Structural Analysis.....	21
11. Fig 4.3: Setup for Modal Analysis.....	21
12. Fig 4.4: Stator and Rotor .....	22
13. Fig 4.5: Stator Mesh and Rotor Mesh.....	22
14. Fig 4.6: Setup for CFX.....	23
15. Fig 5.1: Mesh size v/s Total Deformation.....	24
16. Fig 5.2: Mesh Convergence.....	25
17. Fig 5.3: Mesh Size v/s Number of Elements.....	25
18. Fig 5.4: Total Deformation.....	26
19. Fig 5.5: Equivalent (Von-Mises) Stress .....	26
20. Fig 5.6: Mode Shapes .....	27
21. Fig 5.7: Mode v/s Frequency .....	28
22. Fig 5.8: Residual Plot (Momentum and Mass) .....	29
23. Fig 5.9: Residual Plot (Momentum).....	29
24. Fig 5.10: Pressure Contours.....	33
25. Fig 5.11: Velocity Contours.....	34
26. Fig 5.12: 3-D Stream Lines.....	38
27. Fig 5.13: Turbulence Kinetic Energy Contours.....	40
28. Fig 5.14: Eddy Viscosity Contours.....	41
29. Fig 5.15: Turbulence Eddy Contours.....	43
30. Fig 5.16: Velocity Vector Contours.....	45
31. Fig 5.17: TSR v/s Torque.....	45
32. Fig 5.17: TSR v/s Thrust Force.....	46

## **LIST OF TABLES**

1. Table 1.1: Global Potential of Ocean Energy.....	1
2. Table 4.1: Blade Design Parameters.....	19
3. Table 4.2: Blade Design Details.....	19
4. Table 4.3: Structural Steel Properties.....	20
5. Table 4.4: RPM for Various Respective TSR.....	23
6. Table 5.1: Computational Time.....	28

# CHAPTER-1

## INTRODUCTION

### 1.1 Ocean Energy:

The energy carried by ocean currents, tides, salinity, and temperature fluctuations is referred to as marine energy or marine power (also known as ocean energy, ocean power, or marine and hydrokinetic energy). The flow of water in the world's oceans generates a massive reservoir of kinetic energy or energy in motion. Most of this energy can be used to produce electricity, which can then be used to fuel households, transportation, and factories.

Marine energy refers to both surface wave power and tidal power, derived from the kinetic energy of vast bodies of flowing water. Offshore wind power is not a form of marine energy since wind power is generated from the wind, even though the wind turbines are installed over water.

The oceans provide enormous amounts of resources and are located in much, if not the most, of the world's most densely populated areas. Ocean energy has the ability to generate a significant volume of new renewable energy across the planet.

#### 1.1.1 Global Potential:

Changes in ocean temperatures, salt content, tides, currents, waves, and swells have the potential to generate 20,000–80,000 terawatt-hours a year (TWh/y) of energy.

Energy Form	Annual generation
Tidal Energy	>300TWy
Marine current power	>800TWy
Osmotic power	2,000TWy
Ocean thermal Energy	10,000TWy
Wave Energy	8,000-80,000TWy

Table 1.1: Global Potential of Ocean Energy

## **1.2 Forms of Ocean Energy:**

There are two forms of energy, mainly renewable energy and non-renewable energy. In renewable energy: Marine Current Power, Osmotic Power, Ocean Thermal Energy, Tidal Power, and Wave Energy are present. But the main focus is on Tidal Power.

The energy generated by moving volumes of water, a standard method of generating hydroelectric power. Tidal energy production is classified into three types: tidal stream power, tidal barrage power, and complex tidal power.

## **1.3 Tide:**

Tides are the rise and falling of sea levels caused by the joint gravitational forces of the Moon and Sun, as well as the Earth's rotation. Tide tables can be used to determine the expected times and amplitudes (or “tidal range”) for any given location. Many aspects affect the forecasts, including the Sun-Moon alignment, the phase and amplitude of the tide (deep ocean tide pattern), the amphidromic structures of the seas, and the form of the coastline and near-shore bathymetry. However, these are just predictions; the actual timing and height of the tide are influenced by wind and air pressure. Semi-diurnal tides occur along several shorelines, with two almost identical high and low tides per day. Other places have a diurnal tide, which means there is a high and low tide every day. A “mixed tide” is a third typical type, consisting of two tides of varying magnitudes each day.

Tides differ on timescales ranging from hours to years due to various factors that influence the lunitidal interval. Tide gauges at fixed stations monitor water levels over time and create reliable records. Variations produced by waves of intervals shorter than minutes are ignored by gauges. These values are comparable to a reference (or datum) level known as mean sea level. Although tides are the most common cause of short-term sea-level variations, sea levels are often affected by factors such as wind and barometric pressure changes, which cause storm surges, especially in shallow waters and near coasts.

### **1.3.1 Characteristics:**

Tide variations take place in the following stages:

- Flood tide occurs as the sea level increases for several hours and covers the intertidal plain.
- The sea rises to its highest point, resulting in high tide.

- Ebb tide occurs as the sea level decreases for several hours, exposing the intertidal zone.
- The sea ceases sinking as it reaches low tide.

Tidal streams are the oscillating waves caused by tides. The point at which the tidal current ceases to exist is referred to as slack water or slack tide. The tide then turns in the other direction and is considered to be turning. Slack water is typically found near high and low water levels. However, there are several places where slack tide times vary significantly from high and low water times.

Tides are usually semi-diurnal (two high and two low tides each day) or diurnal (one tidal cycle per day). The two high waters on a given day are also not the same height in tide tables, these are the higher high water and the lower high water. Similarly, the two low waters are the upper low water and the lower low water each day. When the Moon is above the Equator, the regular inequality is inconsistent and relatively minimal.

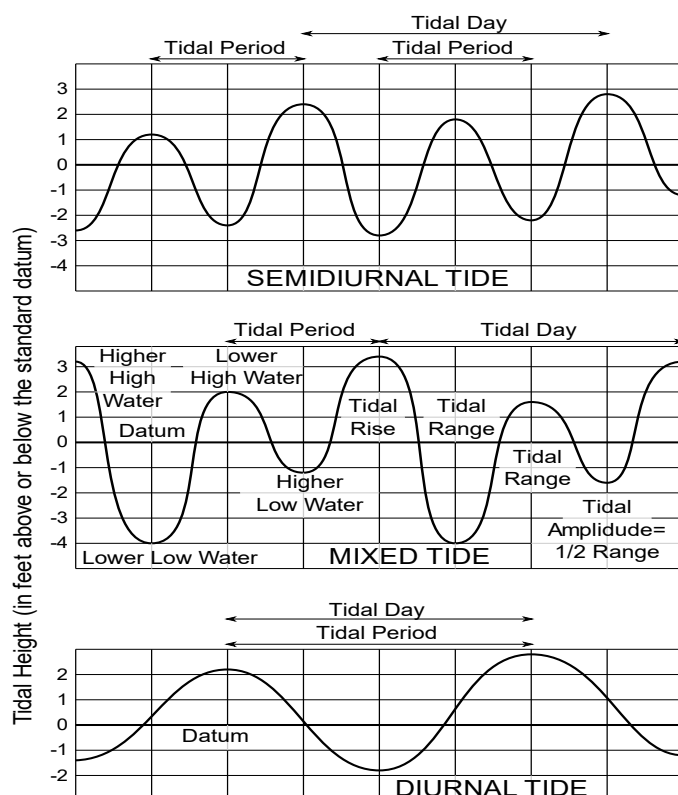


Fig 1.1: Distribution of Tide Phases

### 1.3.2 Definitions:

- Highest astronomical tide (HAT) – The highest tide that can be expected. It should be noted that weather conditions can cause the HAT to rise higher.
- Mean high water springs (MHWS) – The average of two high tides on spring tide days.

- Mean high water neaps (MHWN) – The average of two high tides on neap tide days.
- MSL (mean sea level) – The average sea level. Over a long period of time, the MSL remains constant for every place.
- Mean low water neaps (MLWN) – The average of two low tides on neap tide days.
- Mean low water springs (MLWS) – The average of two low tides on spring tide days.
- Lowest astronomical tide (LAT) and map datum (CD) – The lowest tide that can be expected.

This is used as the chart datum of some charts. It should be noted that under certain meteorological conditions, the water level can drop lower than this, implying that there is less water than seen on charts

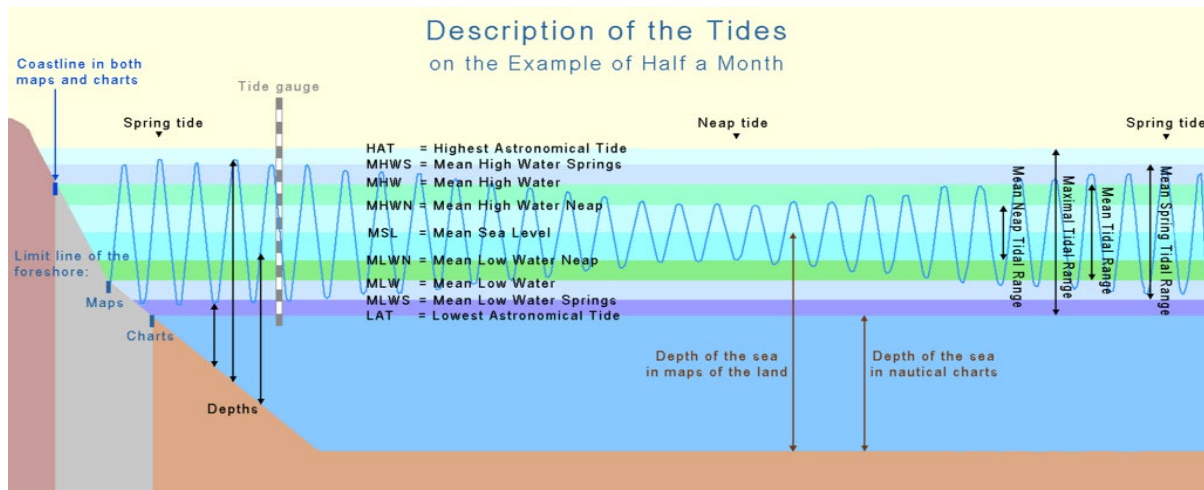


Fig 1.2: Depiction of Various Tides

#### 1.4 Methods to Extract Tidal Energy:

Researchers proposed a variety of methods for extracting tidal energy. However, the fundamental theory behind all the methods remains the same. There are, however, two main techniques for extracting energy from the tides.

- Estuaries, into which vast volumes of seawater flow due to a high tidal range, are captured behind barrages, and turbines spin by using the potential energy of the accumulated water.
- The kinetic energy of flowing water can generate energy in the same way as wind energy can be extracted. All of the strategies listed above have been proposed and used, and each has its own set of benefits and drawbacks (Bryden and Melville, 2004).

It could also be possible to use pumping techniques for barrages to improve performance and help meet energy demand. The equipment used in energy generation differs

in scale, form, and requirements. The systems have been divided into three categories by ISSC (2006):

- Tidal barrages store tidal flow and generate power through discharge.
- Tidal fences obstruct a passage when extracting energy in one or both directions of tidal flow.
- Tidal current machines that are anchored or moored in the middle of a tidal sea.

#### **1.4.1 Tidal Barrages:**

A tidal barrage is a barrier that is typically constructed over the mouth of an estuary from which water flows in and out of the basin. The tidal barrage is equipped with sluice gates that enable water to flow into and out of the basin. During high tide, water floods into the harbour, and it is stored by shutting the sluice gates at the start of low tide. The barrage gates are operated by understanding the location's tidal range and operating them at the appropriate times of the tidal cycle. When the sluice gates are opened at low tide, turbines installed at the gates generate electricity.

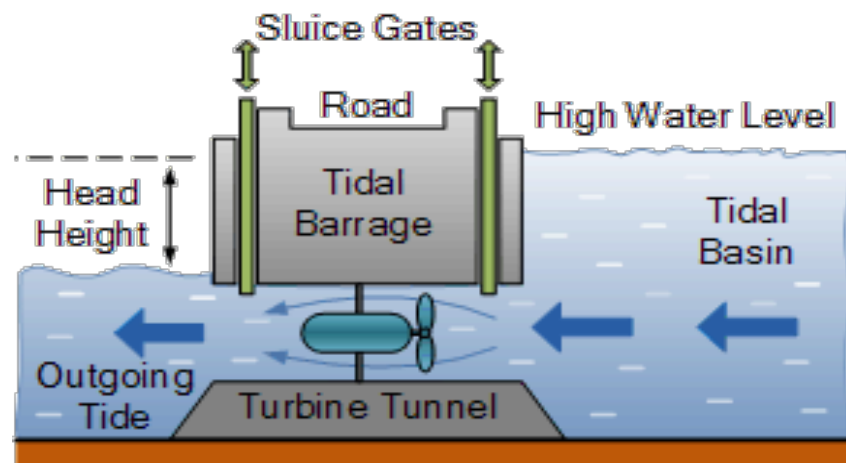


Fig 1.3: Tidal Barrage

#### **1.4.2 Tidal Stream Energy:**

This type of energy uses the kinetic energy of moving water to turn a turbine. The availability of power in the given area is more significant than wind energy since the density of the fluid medium is high. This energy generation tends to be the cheapest and most environment-friendly of any tidal power generation. In this type of energy, Axial turbines and Cross-flow turbines are present.

Axial flow turbines have rotor arrangements parallel to the water stream. This type of turbine is similar to a horizontal axis wind turbine, but some design modification is done to blades due to the difference in the fluid medium. In cross-flow turbines, the rotor is arranged perpendicular to the water stream. This type of turbine is similar to the Darius turbine with some design modifications in the blade. This type of turbine uses the drag of water to generate energy.

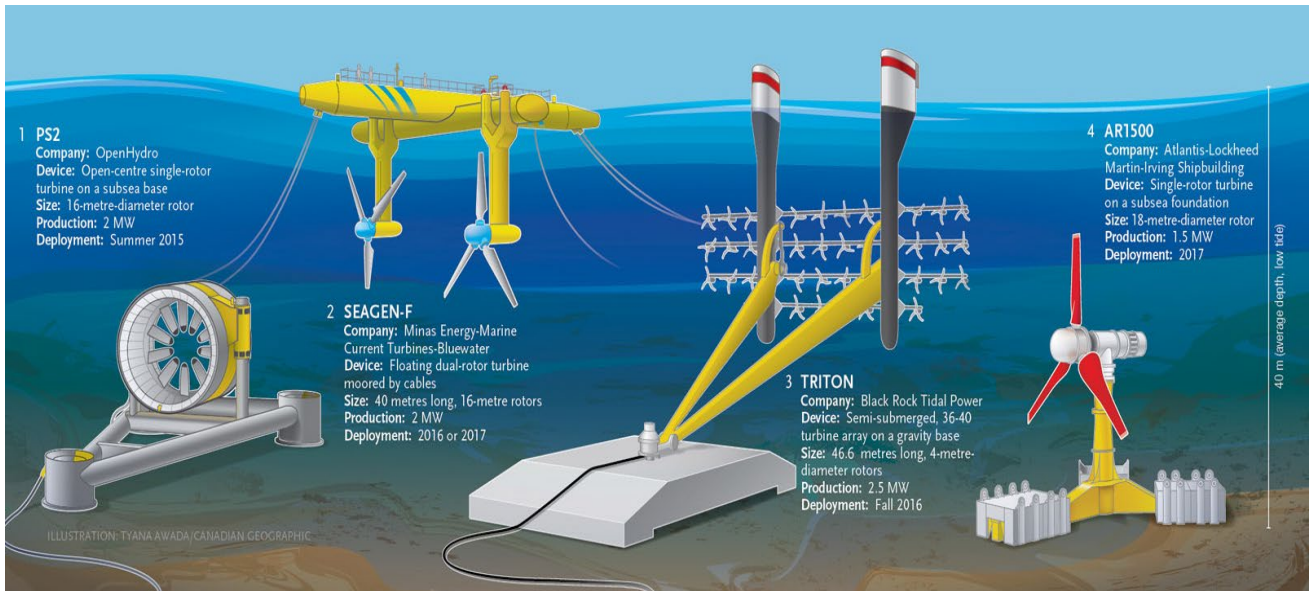


Fig 1.4: Various Tidal Stream Devices

## CHAPTER-2

### LITERATURE REVIEW

#### **2.1 Literature Survey:**

[1] In this paper, a Horizontal Axis Tidal Turbine (HATT) has been chosen. They have used S814 airfoil design to design turbine blades. For this turbine, they have preferred a three-piece blade over a two-piece blade of low start flow velocity, and also because of stable disk characteristics. They first evaluated the site area, including the depth at which it is positioned, and then developed the blade using blade element theory, which was then modelled using CATIA software.

They tried to compare and verify turbine performance measured in the Circulated Water Channel (CWC) experiment and prediction from CFD analysis. After practical examination at the site location, they chose to do with water current velocity taken as 1.0 m/s with a blade diameter of 0.5 m. A CWC has been designed to do CFX flow analysis with a rectangular parallelepiped (stator) of width 1 m, length 4.75 m, height 0.8 m, and the internal rotational element (rotor) with a cylindrical cross-section of diameter 0.5 m and height 0.11 m. In this CWC, the inlet condition is given as 1.0 m/s, the walls and floors of the external domain are given as "wall condition", and the free slip condition is given to the upper side. The frozen rotor condition was used as the interface condition of the internal rotating area and external area. By applying these conditions, torque values were calculated using ANSYS CFX Post-processor.

Since building the turbine, they used an unstructured mesh of tetrahedrons and prisms to mesh it. For this purpose, they created a dense prism-layer mesh around the blade with 2,671,523 elements and 5,65,443 nodes and on the turbine blades with a tetra-prism mesh consisting of 1,69,819 nodes and 9,47,896 elements. The Shear Stress Transport model was used to accurately predict the size and onset of flow peel caused by adverse pressure gradient by calculating the transport of turbulence shearing stress. Since it is simple to extend into an automated wall treatment, the accuracy of the analysis can be obtained regardless of the mesh's  $y^+$ . And then, coming to the simulation part, they simulated flow analysis using ANSYS CFX V11 SP1 software. In CFD analysis to calculate torque value, they have done six analysis results from 2 to 7 tip speed ratio (TSR). In their analysis, the maximum value of the output coefficient is about 0.51 at TSR 5.

After CFD analysis, they have received computed images of Turbulence Kinetic Energy, Streamlines, and mainly pressures acting on the different side of the blade. Since the turbine used in this analysis is a lift type (S814) and uses lift caused by a difference in fluid pressure according to the asymmetric shape of the airfoil. The CFD analysis found that the pressure in the region near the tip and the leading edge continues to increase at the acting face, and at TSR 7, negative pressure occurs at the tip part. Now, at the suction side of the turbine, negative pressure increases continuously up to tip speed ratio 5, and then gradually, the increase in negative pressure slows down. Comparing the acting face side (pressure side) with the suction side, they got about  $4.0 \times 10^4$  pa.

Then, in pressure distribution of blades from the results, they have a gradual pressure increase at the leading edge at the pressure side (acting face side), and the same takes place at a negative pressure of the suction side. At TSR 5, negative pressure occurs on the pressure side of the maximum thickness position, and the pressure difference between the pressure side and suction side also decreases which in turn reduces the lift and torque forces.

The above CFD analysis found that, If the TSR becomes lower than 5, the blade is placed with a greater angle of attack than that of the maximum Lift-Drag ratio. As the angle of attack increases, a stall occurs, and torque is reduced. If the TSR becomes greater than 5, lift decreases, and torque is reduced because the angle of attack becomes smaller than that of the maximum Lift-Drag ratio. The streamline results found that, as TSR increases, the rotor streamline expands to the maximum at a TSR of 5, where maximum efficiency appears. As the TSR increases, it becomes more complicated as the wake caused by the turbine develops faster.

[2] In this paper, they wanted to design a tidal turbine, so they studied and computed several times to get an optimal design for a turbine. For this, they have calculated tangential velocity, tangential flow velocity, overall resultant relative velocity, angle of resultant velocity, lift and drag forces, and mainly axial and tangential forces to design a proper blade. After assessing the site location conditions, they have calculated the desired power to be extracted, and it is around 1.5 MW by using a three-bladed rotor configuration. The regular and extreme flow velocities that a turbine can run are between 2.4 m/s and 4.1 m/s, respectively.

To meet the above requirements, they must have a hydrofoil with a suitable thickness near the blade root to resist the expected high bending moments in the required conditions. These blades must also be insensitive to surface roughness effects for the predicted pressure ratios during normal operating conditions. Also, rotor size and rotational speed affect the rated

power. They have chosen the Riso-A1 family of airfoils that offer high lift-to-drag ratios over a wide angle of attack range by considering the above conditions. Then, the lift coefficient and angle of attack are taken and used as input for the stream-tube model.

In this project, they have followed an iterative process for modeling a turbine. A trial-and-error method was followed to get an optimal design, and this design of blades is kept in a stream tube model for flow velocity calculations. At the site location, the turbine must be installed at 40-50 m below sea level. At this depth, the rotor can have a maximum diameter of 25 m. Since the blades are long, they create significant bending moments at the tip of the blades. By this configuration of the blade, they have a maximum speed of 12 rpm, with a power production target of 1500 kW. A peak efficiency between 8 rpm and 11 rpm was observed using this design.

Now, after this, they have to address cavitation. This cavitation results in a faster wear rate and uncertainty of load acting on the blade, which is an unwanted effect. Thus, this problem needs to be avoided, but these issues are not addressed in BEMT and conventional stream tube models. To rectify this situation, they have incorporated a cavitation check which is helpful for practical examination. After this, they have concluded a blade chord length of 12 m, which is rotating at 10 rpm, is effective. The modeling of the hydrodynamic blade, after it passes each stage on the blade, is an optimal blade of experimentation where Riso-A1 family blades have passed.

For structural modeling, the blade is technically treated as a cantilever beam, and with tangential and thrust forces at each blade station, output from the stream-tube model and edgewise and flatwise bending moment distribution for turbine blade is calculated. The material selection for the blade is the following process, as they need a material with high specific strength and stiffness for the blade to regain its shape under high loading conditions. They also need a material with a negligible corrosion effect under seawater conditions. So only fiber-reinforced polymer composites, specially GFRP and CFRP materials, are commonly employed in wind turbines and used here for construction purposes. This FRP model should be evenly applied due to irregular forces and, if not done correctly, cause damage to blade geometry.

Then, they have analysed by using the finite element method (FEM). Using PreComp, a detailed FEM is developed to get a more accurate strain analysis of the blades. PreComp uses a modified version of traditional 2D laminate plate theory in conjunction with a shear flow

technique to measure the stiffness and inertial properties of the composite blade at discrete points along the blade in a span-wise direction. The whole blade is not handled as a single structure in this process. Instead, it is divided into various sectors. The Leading-edge of hydrofoil is considered as Sector-1, the spar caps at the middle of the blade are considered Sector-2, and finally trailing edge is considered Sector-3. In PreComp, a sector can be defined as a laminate or laminas stack composed of many materials.

Now coming to the finite element model, they have used Autodesk Inventor software which is a modeling tool to create a 3D shell model of the blade. They have taken this 3-D model to the Abaqus 6.9 software finite element program, where analysis has been done after all the boundary conditions on the blade have been applied. This blade has been modelled using 4-Node reduced integration(S4R) linear shell elements with enhanced hour-glass control. This blade design includes a circular transition area from the steel hub to the blade for completeness, although the strain analysis only commences at a distance of 2 m from the hub until the blade's tip.

After inspection of the results, the most significant forces acting on the blade are axial forces that result in flap-wise bending being six times larger than the edgewise moment for the blade length at a speed of 2.4 m/s tidal flow. When these results are compared with PreComp for CFRP blade, good agreement was observed between the models, with the finite element model predicting slightly higher strain values in general. A factor of safety of 1.6 was observed for a CFRP blade under extreme load conditions.

The calculated thickness of the spar caps would require a significant quantity of CFRP, for construction with substantial implications for production costs, compared to GFRP blades. They are supposed to last over 20 years due to the high quality of the construction. Also, for commercial-scale tidal turbines with 12 m length blades, the bending moments predicted by the stream-tube model at normal and extreme loads, have resulted in significant strains in GFRP that would result in fiber failure. Mainly CFRP offered a noticeable improvement in the maximum strain levels, which are below the tensile failure strain of the material used in the model.

[3] This paper discussed the flap influence on a 2-D NACA 4412 airfoil numerically investigated in viscous ground-effect flow. They have used the Spalart-Allmaras turbulence model in the finite volume method. For simulation purposes, they have used ANSYS CFD

Fluent computer program software. They have focused on calculating the effect of angle of attack, flap angle arrangement, aerodynamic forces, and Reynold's number.

Wing-in-Ground (WIG) effect occurs here because the airfoil flies close to the ground and provides beneficial aerodynamic properties. Here to generate lift of the vehicle moving at a low speed or heavy moving vehicle such as big ship, heavy plane, etc., these flaps are arranged at the airfoil's trailing edge to get more lift. So as the wind direction changes, these flaps are adjusted accordingly to it.

They chose NACA 4412 because it has an almost flat bottom surface and prevents negative ground effect. They modified the airfoil (NACA 4412) with plain and split flaps added to the chord length of 80% for experimentation purposes. This is because the plain flap deflects the airfoil trailing edge to the desired position, while split flaps add a thin plate flap beneath the airfoil without any airfoil deflection of the trailing edge.

The numerical model used here has the general equations that govern WIG flow with a flap: the Reynolds Averaged Navier Stokes (RANS), incompressibility, 2-Dimensional, and a constant viscosity. These equations represent laws of conservation of mass and momentum in the computational domain and flow conditions. The meshing used was a C-mesh around the airfoil for fine mesh around the nose for sound quality analysis, and in far regions around the airfoil, an H-mesh is used outside the C-mesh.

They applied a no-slip wall condition at the ground with fluid moving with free stream velocity for boundary conditions. The top boundaries and upstream are given as velocity inlets at the free stream conditions, and at downstream, they have given pressure outlet. Finally, a no-slip wall is applied airfoil surface. The results show that:

- The Aerodynamic coefficient is close in free air flight.
- Due to deflection by the flaps, the flow was trapped beneath the airfoil, which results in flow velocity reduction and pressure building up under the airfoil.
- As flap attack angle increases, lift and drag increases
- Since flaps are deflected, the drag coefficient increases significantly. With minute deflection in the flap, the lift-to-drag ratio is augmented substantially.
- Any changes in Reynold's number have minimal effect on addition in the flap in extreme ground effect.

## **2.2 Motivation for the Present Work:**

Tidal energy is extracted from oceanic tides into electric power using various methods. Among all renewable energy sources such as Wind energy, Solar energy, and Geothermal energy, etc, comparatively tidal energy has relatively high capital costs and only a few potential sites to extract energy. But the benefit it has that the tides can be predicted more accurately than sun and wind resources.

The main benefit of tidal energy is its efficiency. Almost 80% of the tidal energy can be captured to generate electricity. It is more energy secure than other renewable energy extraction sources, as it is naturally available and has no harmful greenhouse gas emissions.

With more technological advancements and different blade designs coming into the market, the productivity of energy extraction has increased rapidly in many countries. India is a developing country, and the electricity demand is rapidly growing year by year. According to International Energy Agency (IEA), demand has drastically increased between 1990 and 2017, with electrical energy accounting for around 40% of the total energy utilised in 1990, and that number is expected to rise to 50% in 2030.

By using tidal energy, there is an increased demand of 16% in 2018 and 13% in 2019. More research is happening in technological advancements for various aspects, such as reducing running cost and large development programmes being planned. The world's first large-scale tidal power plant is in France, named Rance Tidal Power plant, operating from 1966. After this, another big power plant has come into operation in South Korea called Sihwa Lake Tidal power station operating from August 2011. This Sihwa station used a tidal barrage system with ten turbines generating 253 MW of power output.

# CHAPTER-3

## OBJECTIVES AND METHODOLOGY

### **3.1 Objectives:**

To design a tidal turbine, which is sustainable at 120 m depth of seawater, and extract maximum available energy to produce electricity.

### **3.2 Methodology:**

- Calculating Rated Power of Turbine by using Betz limit method.
- Designing the Turbine Blade using Blade Element Momentum Theory (BEMT).
- Finding Maximum Deformation and Stress on Tidal Turbine from Static Structural Analysis by assuming Turbine Blade as a Cantilever Beam.
- Finding the natural frequencies for different modes of the Tidal Turbine from Modal Analysis by assuming Turbine Blade as a Cantilever Beam.
- Calculating Desired Boundary Conditions for Flow Analysis using Tides Equation.
- Calculating Thrust force & Torque from Flow Analysis using Computational Fluid Dynamics (CFD).
- Optimizing operating conditions for Maximum Torque from Tip Speed Ratio (TSR) v/s Torque Curve.

#### **3.2.1 Betz Limit Theory:**

The Betz limit is the theoretical maximum efficiency for a wind turbine proposed in 1919 by German physicist Albert Betz. He determined that this value is 59.3 %, implying that only 59.3 % of the wind's kinetic energy will be used to rotate the turbine and produce power. In practice, turbines cannot meet the Betz cap, and typical efficiencies vary from 35-45 %.

This theory is commonly applied to wind turbines to determine how much kinetic energy from the wind can rotate the turbine and produce electricity. The same approach can be used to calculate how much kinetic energy from tides can spin the turbine and produce electricity, with the distinct difference being a variation in fluid density and extraction of kinetic energy.

$$E_c = \frac{1}{2} \rho V v^2 [Nm \text{ or joules}]$$

$$V = A v \left[ \frac{m^3}{s} \right]$$

$$P = \left( \frac{\rho \pi D^2 U^3}{8} \right) [W]$$

$$P_{expect} = \eta C_p \left( \frac{\rho \pi D^2 U^3}{8} \right) [W]$$

### 3.2.2 Blade Element Momentum Theory (BEMT):

The angular momentum of the rotor is accounted for by the blade element momentum theory. In figure 3.1, there is a stream tube containing the fluid and the rotor. It can be presumed that the contents of the stream tube have no contact with anything outside of it. That is, it is treated as working with an isolated system. The conservation of angular momentum, which in this case, in the flux tube must then be conserved. As a result, if the rotor gains angular momentum due to its contact with the fluid, everything else would gain equal and opposite angular momentum.

Since the device is made up of just the fluid and the rotor, the fluid must gain angular momentum in the wake. The change in angular momentum of the fluid is linked to the tangential induction component,  $a'$ , similar to the change in axial momentum with some induction factor  $a$ .

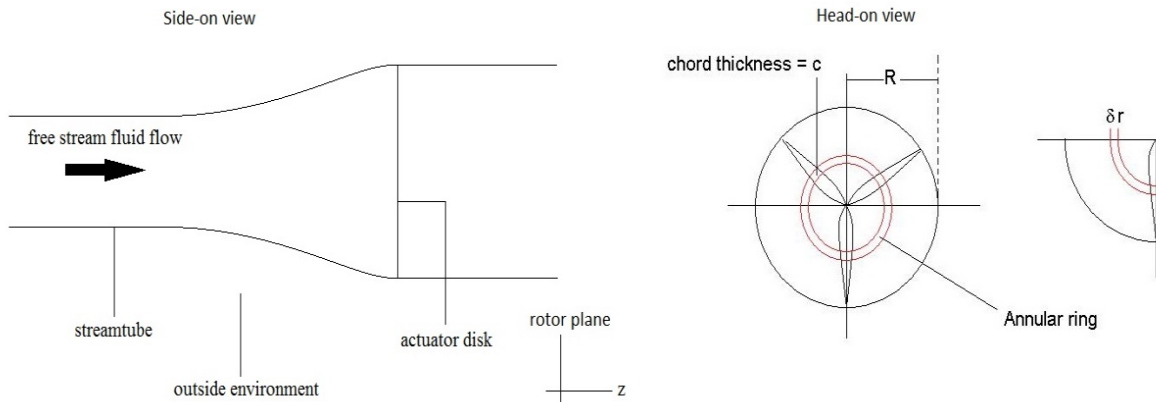


Fig 3.1: Blade Element Momentum Demonstration

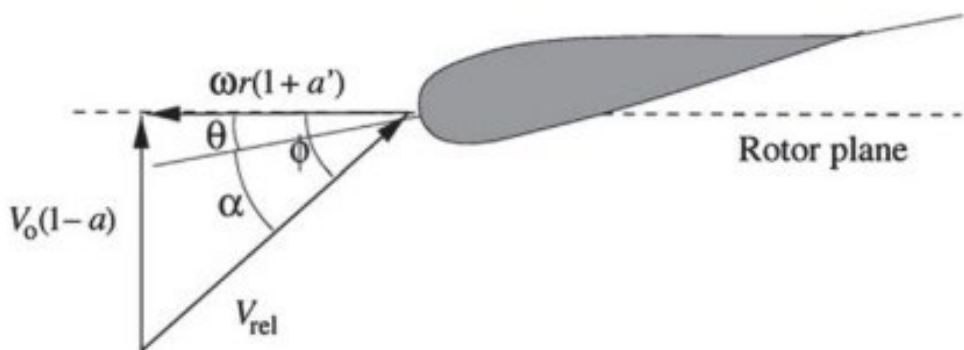


Fig 3.2: Blade Element Momentum Method for Designing Blade

The rotor area would be divided into annular rings of infinitesimally small thickness. This is done to conclude that the axial and tangential induction variables are stable in the annular ring. This approach assumes that annular rings are independent of one another, i.e., that there is no interference between the fluids of neighbouring annular rings.

$$a = \frac{1}{\frac{4\sin^2\phi}{(\sigma C_N)} + 1} \quad a' = \frac{1}{\frac{4\sin\phi\cos\phi}{\sigma C_r} - 1} \quad \theta = \theta_p + \beta$$

$$\alpha = \phi - \theta \quad \sigma = \frac{cB}{2\pi r}$$

$$C_T = C_L \sin\phi - C_D \cos\phi \quad C_H = C_L \cos\phi + C_D \sin\phi$$

$$\phi = (2/3)\tan^{-1}(1/\lambda_r) \quad c = \frac{8\pi r}{BC_L}(1 - \cos\phi)$$

$$\lambda_r = \sin\phi(2\cos\phi - 1)/[(1 - \cos\phi)(2\cos\phi + 1)]$$

Where,  $\beta$  = twist angle of blade  $\alpha$  = angle of attack

$\theta$  = difference between pitch angle and angle of attack  $\theta_p$  = pitch angle

$\phi$  = inflow angle  $\sigma$  = solidity number

$a$  = axial induction factor  $a'$  = radial induction factor

$c$  = chord length  $B$  = number of blades

$r$  = radius of disc  $C_r$  = coefficient of tangential force

$C_N$  = coefficient of normal force  $\lambda$  = tip speed ratio

$\lambda_r$  = local tip speed ratio

### 3.2.3 Static Structural Analysis:

The estimation of the impact of loads on physical systems and their elements is known as structural analysis. All structures that must sustain loads, such as homes, bridges, aircraft, and vehicles, are subject to this method of study. The structural analysis uses applied dynamics, materials science, and applied mathematics to compute the deformations, internal forces, strains, support reactions, accelerations, and stabilization of a system. The analysis findings are used to validate the fitness of a structure for operation, also preventing physical checks. Structural analysis is, therefore, an essential aspect of structural engineering design.

### 3.2.4 Cantilever Beam:

A cantilever beam is a rigid structural structure supported at one end and free at the other. Cantilever beams may be made of concrete or steel, with one end cast or attached to a vertical support. It is a horizontal beam arrangement with a free end that is subjected to vertical loads.

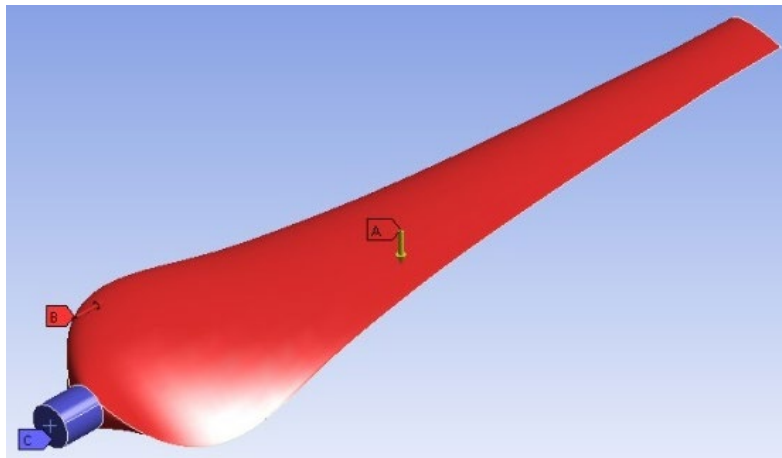


Fig 3.3: Blade as Cantilever Beam for Static Structural Analysis

The blue-coloured region in Fig 3.3 is the fixed support region, which has fixed support, and the other end is left free to be a cantilever beam. The blade has been assumed as a cantilever beam in the analysis.

### 3.2.5 Finite Element Analysis:

Approximate solutions of differential equations are commonly used as the foundation for structural analysis. This is generally accomplished by the use of numerical approximation techniques. The Finite Element Method (FEM) is the most widely used numerical approximation in structural analysis. It approximates a design as an assembly of elements or components connected by different means of attachments, each of which has an associated stiffness. Thus, a continuous system, such as a plate or shell, is represented as a discrete system with a finite number of elements interconnected at a finite number of nodes, and the overall stiffness is the sum of the stiffness of the various elements. Individual element behaviour is described by the stiffness (or flexibility) relationship.

### **3.2.6 Modal Analysis:**

The study of the dynamic properties of structures in the frequency domain is known as modal analysis. Modern experimental modal analysis systems are made up of:

- Sensors such as transducers (accelerometers and load cells, etc.) or non-contact through a Laser vibrometer or stereophotogrammetric cameras.
- Data collection system and an analog-to-digital converter front end (to digitise analogue instrumentation signals)
- Host PC (personal computer) to display and analyse the data.

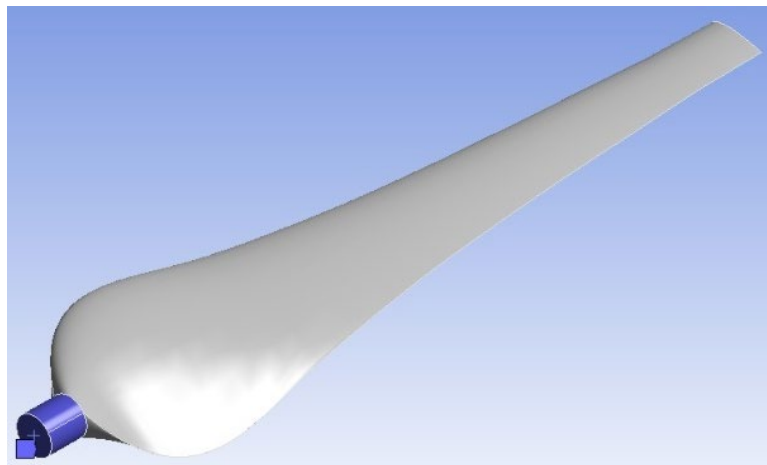


Fig 3.4: Blade as Cantilever Beam for Modal Analysis

The blue colour area in Fig 3.4 represents the structure's fixed support region. As a result, it can be treated as a cantilever beam. So, in this analysis, various vibration modes identical to cantilever beam vibration modes were studied. In this modal analysis, the overall mass and stiffness of the system are used to determine which modes of vibration it would naturally resonate at.

### **3.2.7 Computational Fluid Dynamics (CFD):**

CFD is a subset of fluid mechanics that evaluates and solves problems involving fluid flows using numerical analysis and data structures. The simulations used to model the fluid's free-stream flow and interaction with surfaces defined by boundary conditions are done on computers. Better solutions can be found with high-speed supercomputers, which are often used to solve the most significant and challenging problems. Ongoing study results in applications that increase the precision and speed of complex simulation scenarios like transonic or turbulent flows.

### 3.2.8 Finite Volume Method (FVM):

FVM is a popular approach in CFD codes because it has advantages in memory use and solution speed, particularly for complex problems, high Reynolds number turbulent flows, and source term dominated flows (like combustion).

In the finite volume system, the governing partial differential equations (typically the Navier-Stokes equations, mass and energy conservation equations, and turbulence equations) are recast in a conservative form and solved over discrete control volumes. Using this discretization, a fixed control volume guarantees flux retention. The finite volume equation produces the following governing equations:

$$\frac{\partial}{\partial t} \iiint Q \, dV + \iint F \, dA = 0,$$

where  $Q$  is the conserved variable vector,  $F$  is the flux vector (from Euler equations or Navier–Stokes equations),  $V$  is the control volume element's volume, and  $A$  is the control volume element's surface area.

### 3.2.9 Shear Stress Transport (SST):

SST model is used in the simulation since the tidal turbine is a rotating machinery in a fluid. Menter's Shear Stress Transport turbulence model, or SST, is a popular and reliable two-equation eddy-viscosity turbulence model in CFD. The model incorporates the k-omega turbulence model and the K-epsilon turbulence model, with the k-omega used in the inner boundary layer and the k-epsilon used in free shear flow.

$$\begin{aligned} \frac{\partial(\rho k)}{\partial t} + \frac{\partial(\rho u_j k)}{\partial x_j} &= P - \beta^* \rho \omega k + \frac{\partial}{\partial x_j} \left[ (\mu + \sigma_k \mu_t) \frac{\partial k}{\partial x_j} \right] \\ \frac{\partial(\rho \omega)}{\partial t} + \frac{\partial(\rho u_j \omega)}{\partial x_j} &= \frac{\gamma}{\nu_t} P - \beta \rho \omega^2 + \frac{\partial}{\partial x_j} \left[ (\mu + \sigma_\omega \mu_t) \frac{\partial \omega}{\partial x_j} \right] + 2(1 - F_1) \frac{\rho \sigma_\omega}{\omega} \frac{\partial k}{\partial x_j} \frac{\partial \omega}{\partial x_j} \end{aligned}$$

## CHAPTER-4

### NUMERICAL ANALYSIS

#### **4.1 Blade Element Momentum Analysis:**

The process for designing ideal wind turbine blades is as follows: The blade diameter was determined to be  $D = 2$  m, and the best tip speed ratio was determined to be  $= 5$ . The airfoil style NACA 4412 was chosen for the wind turbine blade design. After calculating the angle of attack to be  $= 5.25^\circ$ , the blade was divided into nine parts. For each segment, the inflow angle and chord length were determined. Finally, each section's twist angle was determined. The following tables list the rotor blade and wind turbine parameters.

Parameter	Blade
Diameter of Blade	2 m
Number of Blades	3
Airfoil type	NACA 4412

Table 4.1: Blade Design Parameters

Section	r/R	Chord Length (m)	Twist Angle (deg)
1	0.2	0.213	24.75
2	0.3	0.181	17.21
3	0.4	0.151	12.46
4	0.5	0.127	9.28
5	0.6	0.11	7.04
6	0.7	0.096	5.38
7	0.8	0.085	4.11
8	0.9	0.076	3.1
9	1	0.069	2.29

Table 4.2: Blade Design Details

## 4.2 Static Structural Analysis:

For doing static structural analysis for the blade, it has been assumed to be a cantilever beam. First, a material is to be assigned to the 3d object, and Structural Steel has been chosen for this purpose. The properties of the material are given in the table below.

Parameter	Value
Density	7850 kg/m <sup>3</sup>
Young's Modulus	200 GPa
Poisson's Ratio	0.3
Bulk Modulus	166 GPa
Shear Modulus	76 GPa
Tensile Yield Strength	250 MPa
Tensile Ultimate Strength	460 MPa

Table 4.3: Structural Steel Properties

Then, at one end, where the blades are placed on the turbine hub, a fixed boundary condition is applied. The nodal displacement will be zero at that point. Next, a gravitational load is applied to the body to examine the effect of gravity on the blade. And it is known that centrifugal force acts in a direction opposite to rotation. Since, the combined effect of centrifugal and gravitational force on the blade is to be calculated, a force component of 1350 N is applied to the blade section normal to the rotational force.

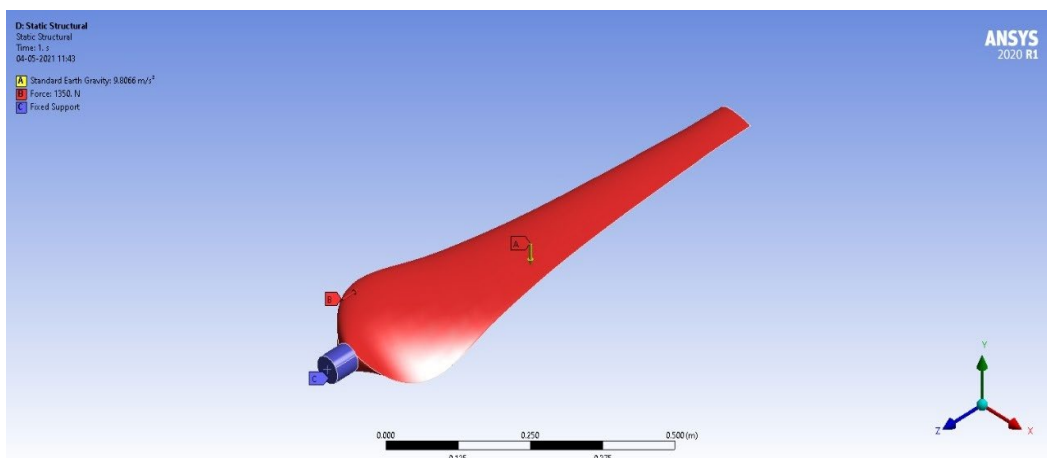


Fig 4.1: Setup for Static Structural Analysis

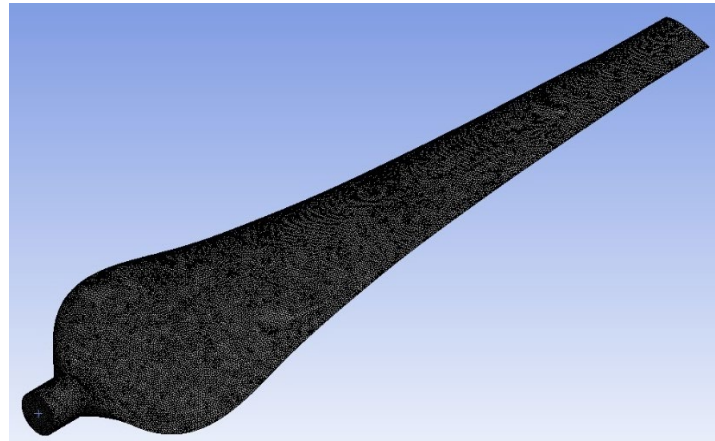


Fig 4.2: Mesh for Static Structural Analysis

Following that, a mesh convergence analysis was conducted to determine the best mesh quality and accuracy. There are 1341937 nodes and 937520 elements in the mesh. The body sizing for the mesh is 0.0025 m. Detailed results are shown in the results section.

#### 4.3 Modal Analysis:

For doing modal analysis for the blade, it has been assumed to be a cantilever beam. This helps in knowing various modes of vibration and the natural frequencies associated with those modes. The pre-stress model is not used because of the computational time constraints. One end of the blade must be fixed, and the region where the blade is placed on the hub to examine various modes of vibration.

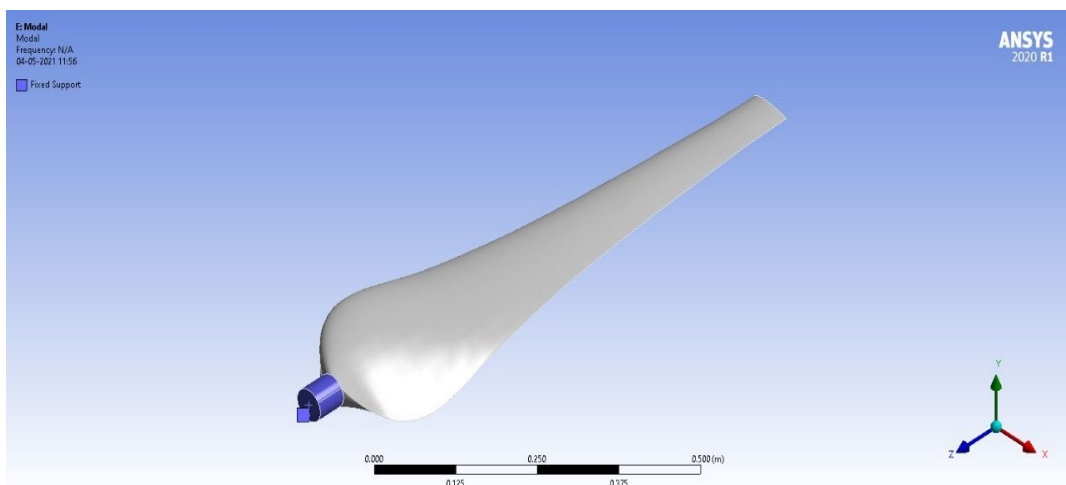


Fig 4.3: Setup for Modal Analysis

After that mesh convergence study was done to find the best mesh quality and accurate results. The mesh consists of 1341937 nodes and 937520 elements. The body sizing for the mesh is 0.0025 m. The input of no. of nodes is needed for the results for which the value 6 is chosen. Detailed results are provided in the results section.

#### 4.4 Flow Analysis:

By doing CFD analysis, a rotor and stator are needed. The rotor region is created with a diameter of 2.05 m and a length of 0.2 m, whereas, for the stator region, a 4x4 square region is created. From the front of the blade, the distance to the square region is 5 m, while from the rear, it is 10 m.

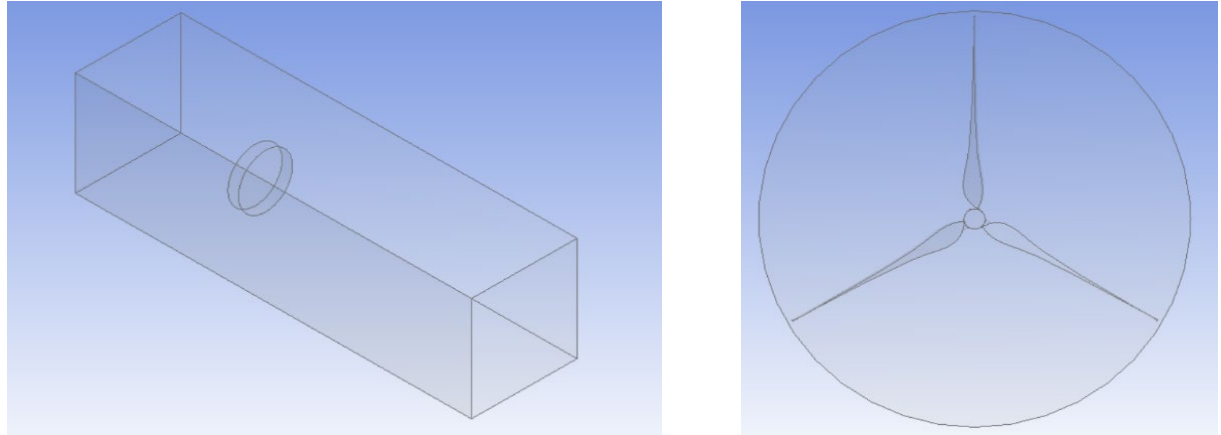


Fig 4.4: Stator (Left) And Rotor (Right)

After that mesh convergence study was done to find the best mesh quality and accurate results. The mesh consists of 4876284 nodes and 3509742 elements for the stator, while for rotor mesh, there are 3480643 nodes and 1766689 elements. A 0.85 mesh quality is achieved for both meshes.

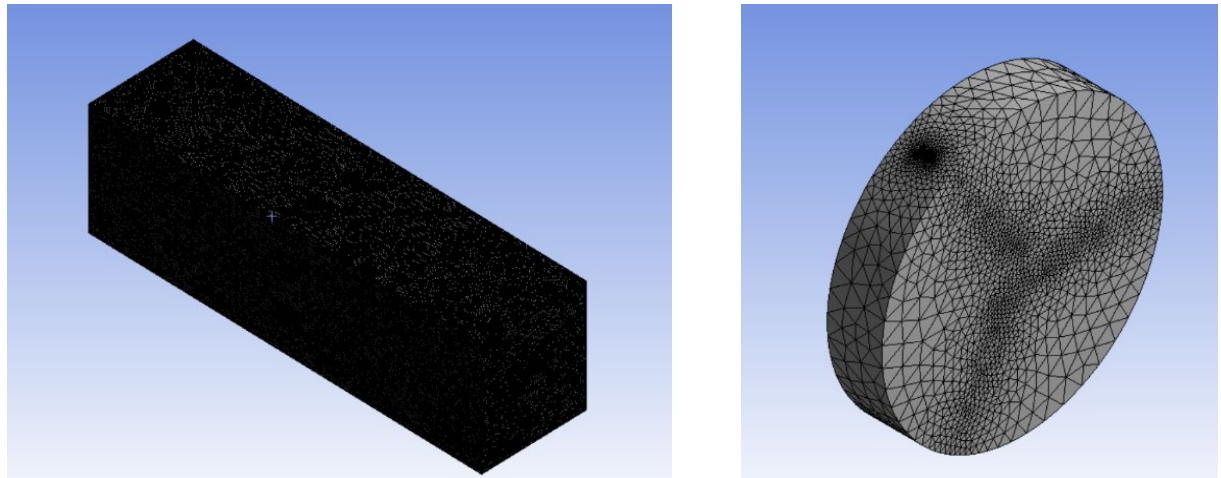


Fig 4.5: Stator Mesh (Left) And Rotor Mesh (Right)

The mesh data has been transferred to CFX for flow analysis setup. The 3D object's front face is called "inlet," and the back face is named "outlet." The top-to-bottom and left-to-right faces were dubbed 'symmetry'. The interfaces between the stator and rotor regions have

been termed "fluid interfaces." The blades and hub were given the names "blades" and "hub," respectively. The following were the setup conditions:

1 m/s for inlet, which is the current velocity, while the outlet is 12 bar pressure, is the pressure at 120 m depth of water. The blades and hub are given "wall", and a no-slip condition is given. Symmetry condition is given for top-bottom and left-right faces. The input for a rotor region is taken by calculated rpm from TSR given in table 3. SST turbulence model is used in this analysis.

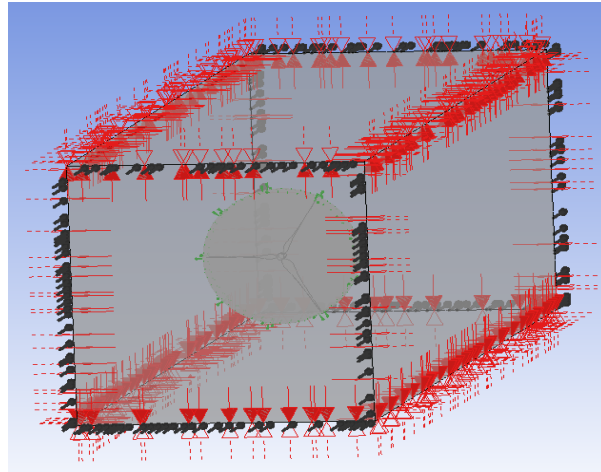


Fig 4.6: Setup for CFX

TSR	R (m)	U (m/s)	Omega (rad/s)	RPM
1	1	1	1	9.5493
2	1	1	2	19.0986
3	1	1	3	28.6479
4	1	1	4	38.1972
5	1	1	5	47.7465
6	1	1	6	57.2958
7	1	1	7	66.8451
8	1	1	8	76.3944
9	1	1	9	85.9437
10	1	1	10	95.493

Table 4.4: RPM for Various Respective TSR

## CHAPTER-5

### RESULTS AND DISCUSSIONS

#### **5.1 Static Structural Analysis Results:**

For better accuracy in the result, a mesh convergence study was done. The first mesh convergence is a graph between mesh size v/s total deformation. The results show that it is in a sinusoidal curve manner. The maximum total deformation at final mesh with 0.0065 elements with a total deformation of -0.00041212.

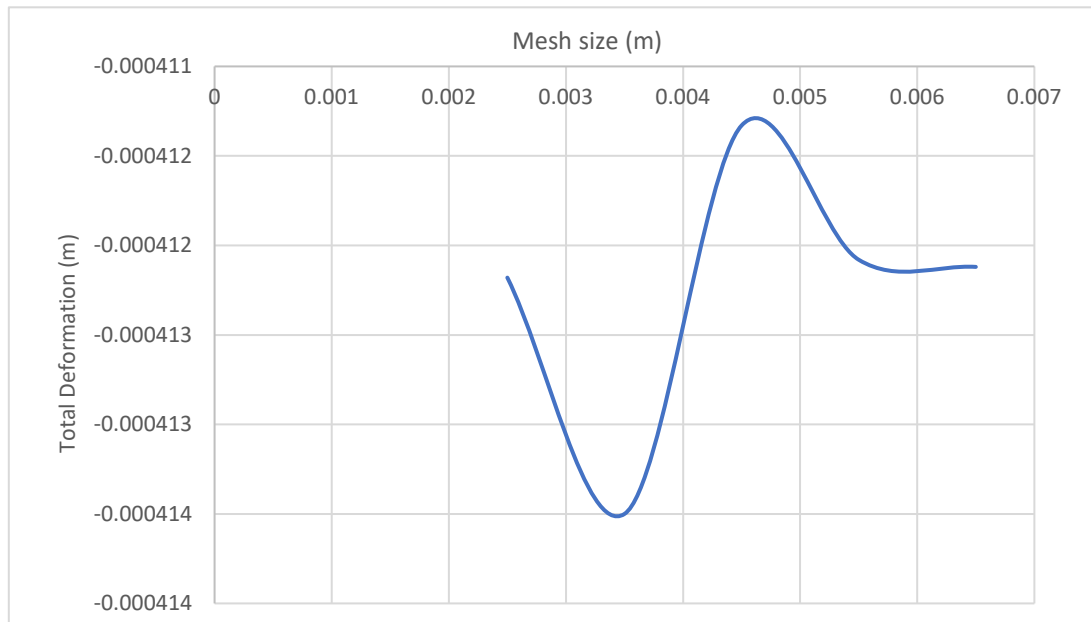


Fig 5.1: Mesh size v/s Total Deformation

In the graph between the number of elements v/s total deformation, an increase is seen, in converge from 1st point with 16,261 number of elements with -0.00041218 of total deformation to 2nd point with 46,833 number of elements with -0.00041133 of total deformation, which is a very slight increase.

From this point, the convergence curve has decreased at a constant rate till 4th point in the curve with 95,082 number of elements with -0.00041208 of total deformation from the graph shows a linear line in a curved manner because there are no points in between till the last point with 9,37,520 number of elements with -0.00041212 of total deformation.

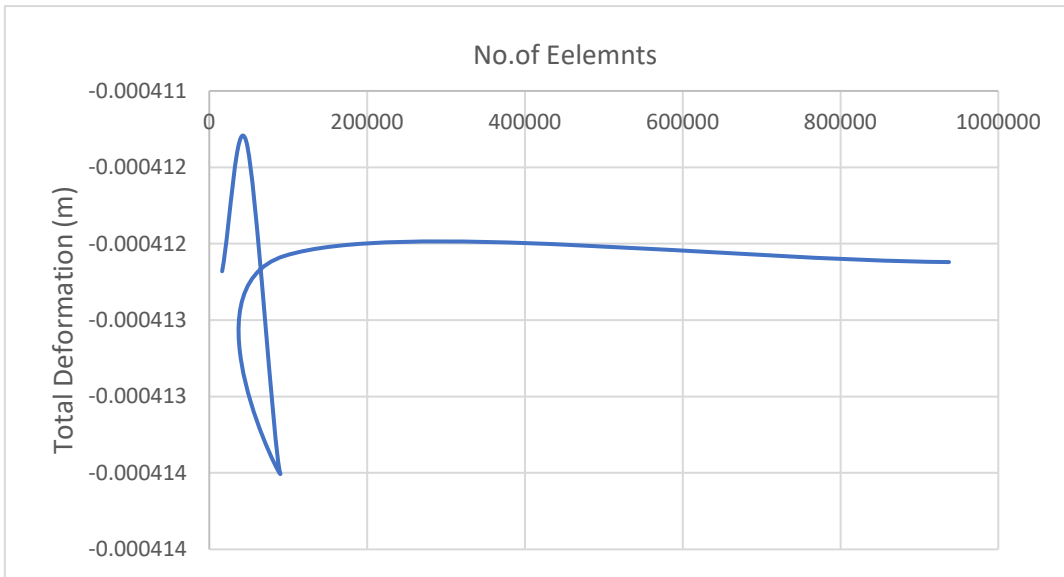


Fig 5.2: Mesh Convergence

In the final graph in this analysis, with Mesh Size v/s No. of elements. This graph shows there is a linear increase from the first point till the last point. But at the 3rd point in the graph with a mesh size of 0.0045 with a total deformation of 46833. After this point, a linear increase until the final point in the graph with mesh size of 0.0065 and a total number of elements of 9,37,520 is seen.

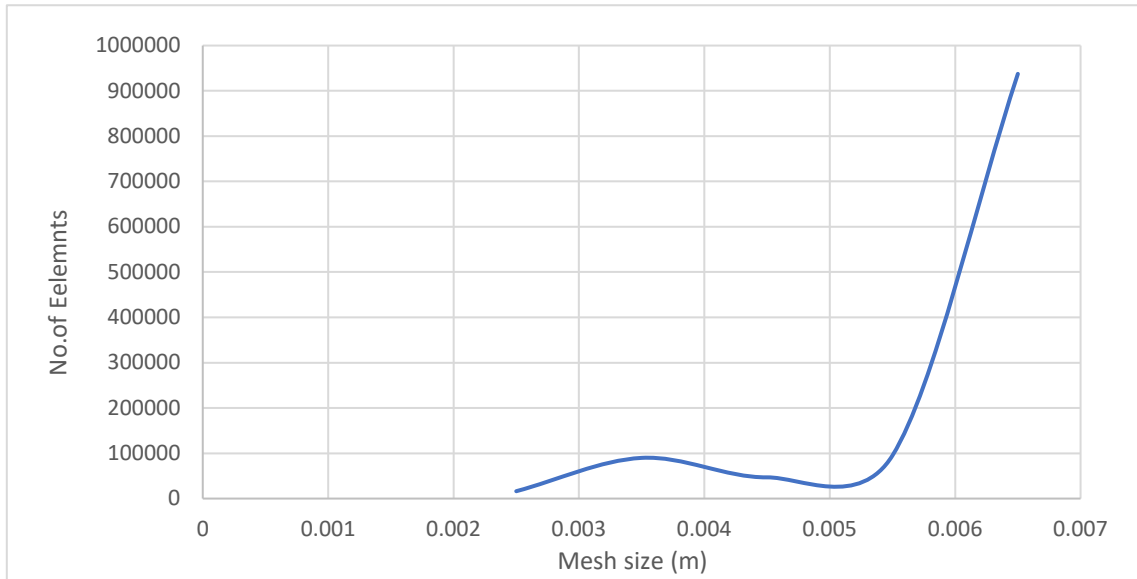


Fig 5.3: Mesh Size v/s Number of Elements

In the computational results image, in the static structural analysis, the blade is assumed as a cantilever beam, at the blade contact point with hub is given as fixed support region and other is left free. The first result is Total deformation. In this, the maximum deformation of 0.00041218 meters is near the tip of the blade design.

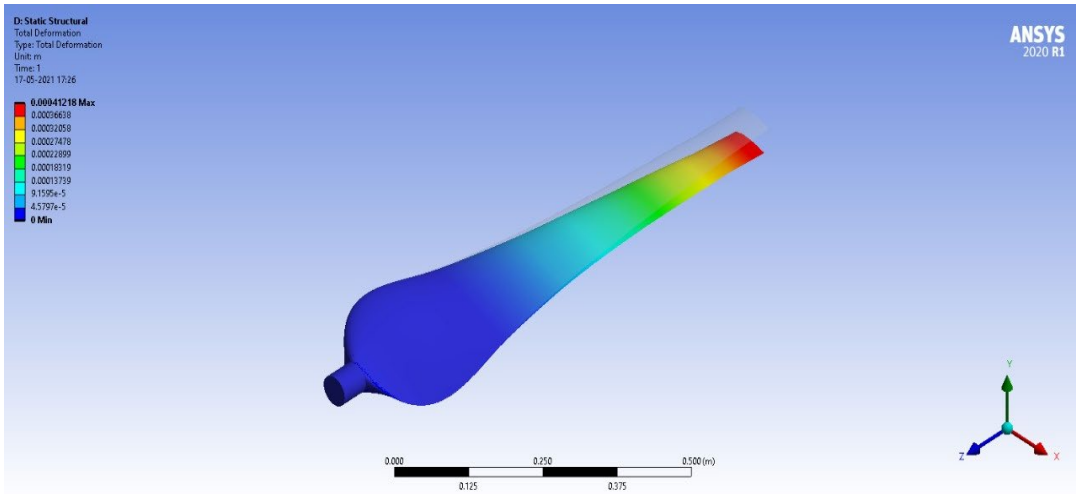


Fig 5.4: Total Deformation

In the static structural analysis, Equivalent (von-mises) stress is computed to check whether the blade falls under the maximum stress limit. In this analysis, stress near the hub and blade contact of the blade is shown in the below figures with 9.0631 MPa maximum stress and minimum stress of 17.407 Pa. Due to the applied load, the bending of the blade near the tips of the blade is shown in the below figures.

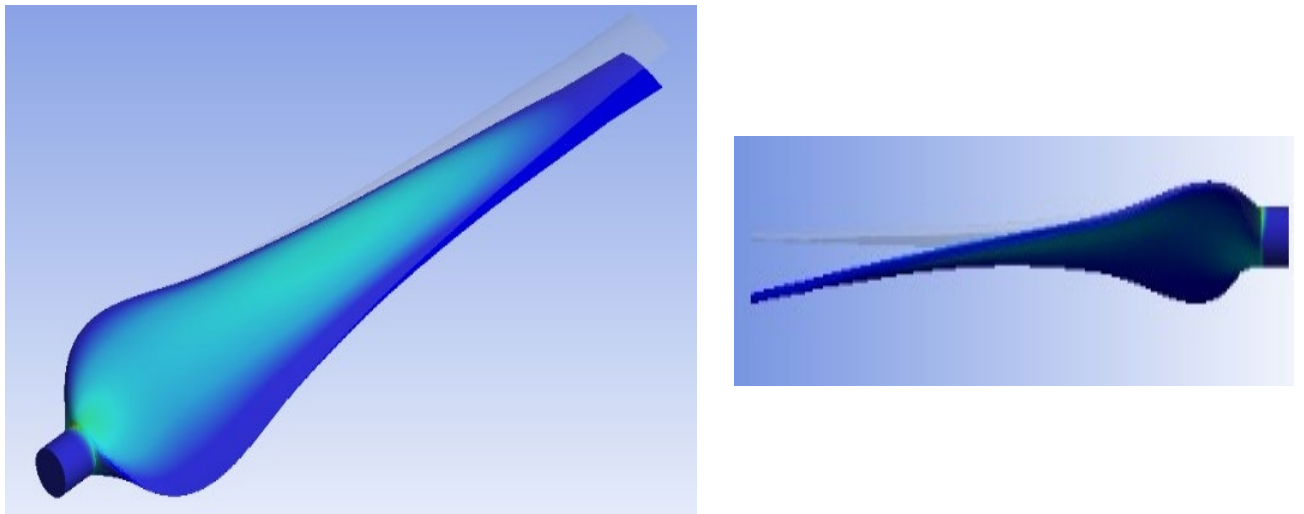


Fig 5.5: Equivalent (Von-Mises) Stress

## 5.2 Modal Analysis Results:

There are three types of vibrations in a cantilever beam, which can be seen in the following results. They are Edge bending mode, Flexural mode, and Torsional mode of vibration. This analysis shows whether the blade vibration is not matching with excitation frequency for resonance.

In the results, the 1<sup>st</sup> and 2<sup>nd</sup> mode show edge bending mode of vibration, and the 3<sup>rd</sup>, 4<sup>th</sup> and 5<sup>th</sup> mode shows the flexural mode of vibration, while the 6<sup>th</sup> mode shows the Torsional mode of vibration.

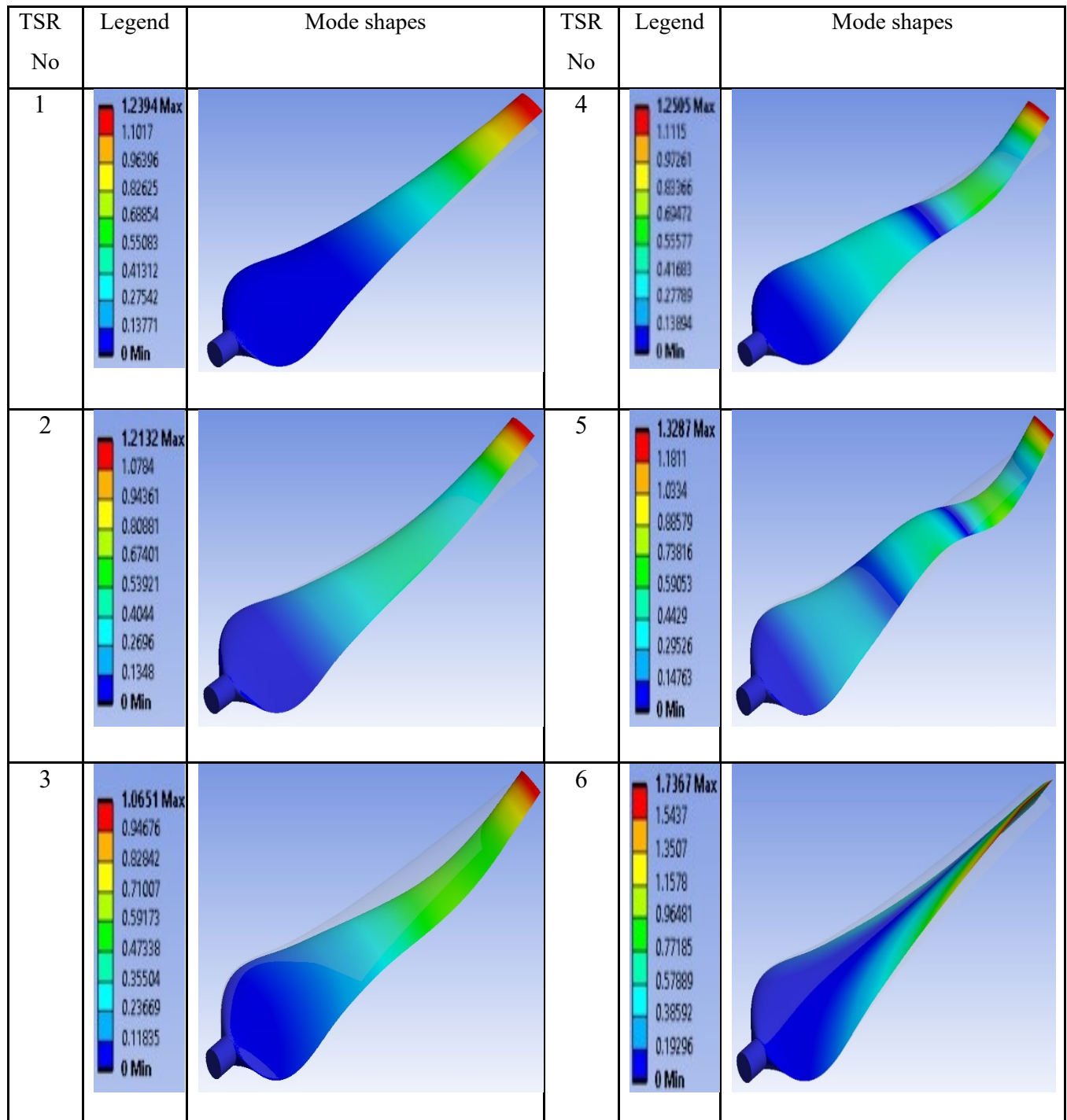


Fig 5.6: Mode Shapes

In this analysis, a graph between Mode v/s Frequencies is produced. The graph below shows there is a linear increase from 1<sup>st</sup> to 4<sup>th</sup> mode, and from 4<sup>th</sup> to 5<sup>th</sup> mode, there is a rapid

increase, and from 5th mode to the last 6th mode, there is a linear increase. The range of mode frequency is 33.617 Hz to 469.95 Hz.

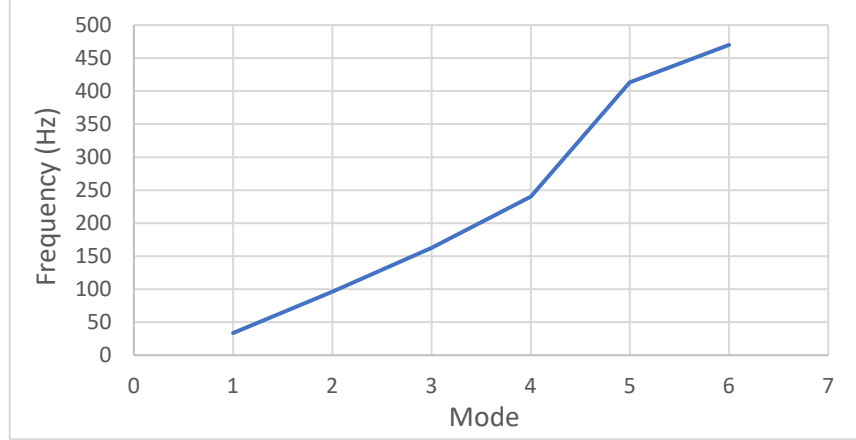


Fig 5.7: Mode v/s Frequency

### 5.3 Flow Analysis Results:

In this flow analysis, the simulation is done from TSR1 to TSR10, and the details of the numerical simulation are shown below. The total simulation has taken approximately five days.

Tip speed ratio (TSR)	Time	Iterations
1	1 hours: 2 min: 58.096 sec	45
2	2 hours: 40 min: 18.805 sec	122
3	5 hours: 31 min: 13.725 sec	250
4	8 hours: 41 min: 20.306 sec	386
5	10 hours: 52 min: 58.802 sec	498
6	13 hours: 56 min: 56.471 sec	626
7	16 hours: 8 min: 16.805 sec	739
8	18 hours: 32 min: 12.083 sec	838
9	20 hours: 23 min: 41.791 sec	918
10	20 hours: 38 min: 14.265 sec	955

Table 5.1: Computational Time

The below residual plots show the Mass & Momentum and the Turbulence (KO) for TSR 5.

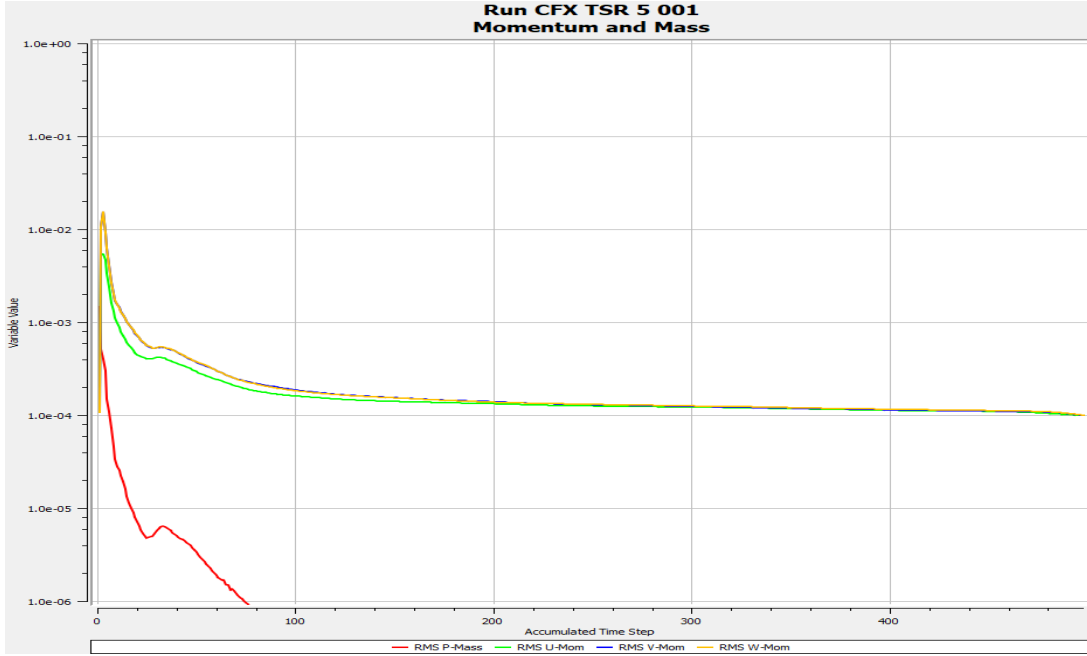


Fig 5.8: Residual Plot (Momentum and Mass)

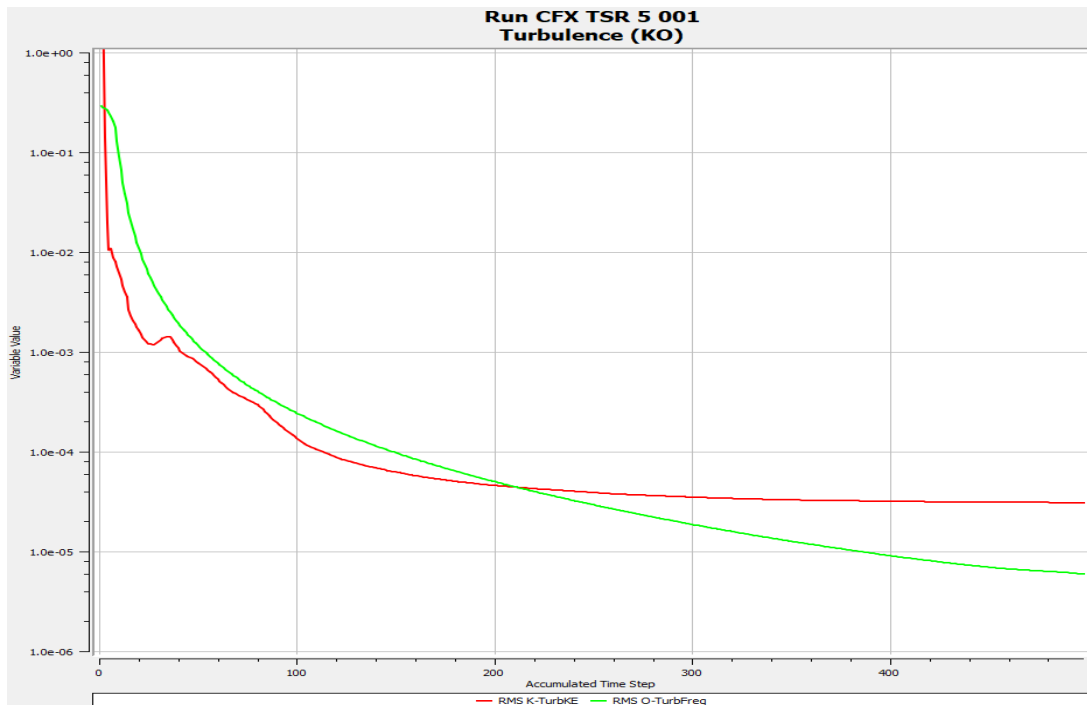
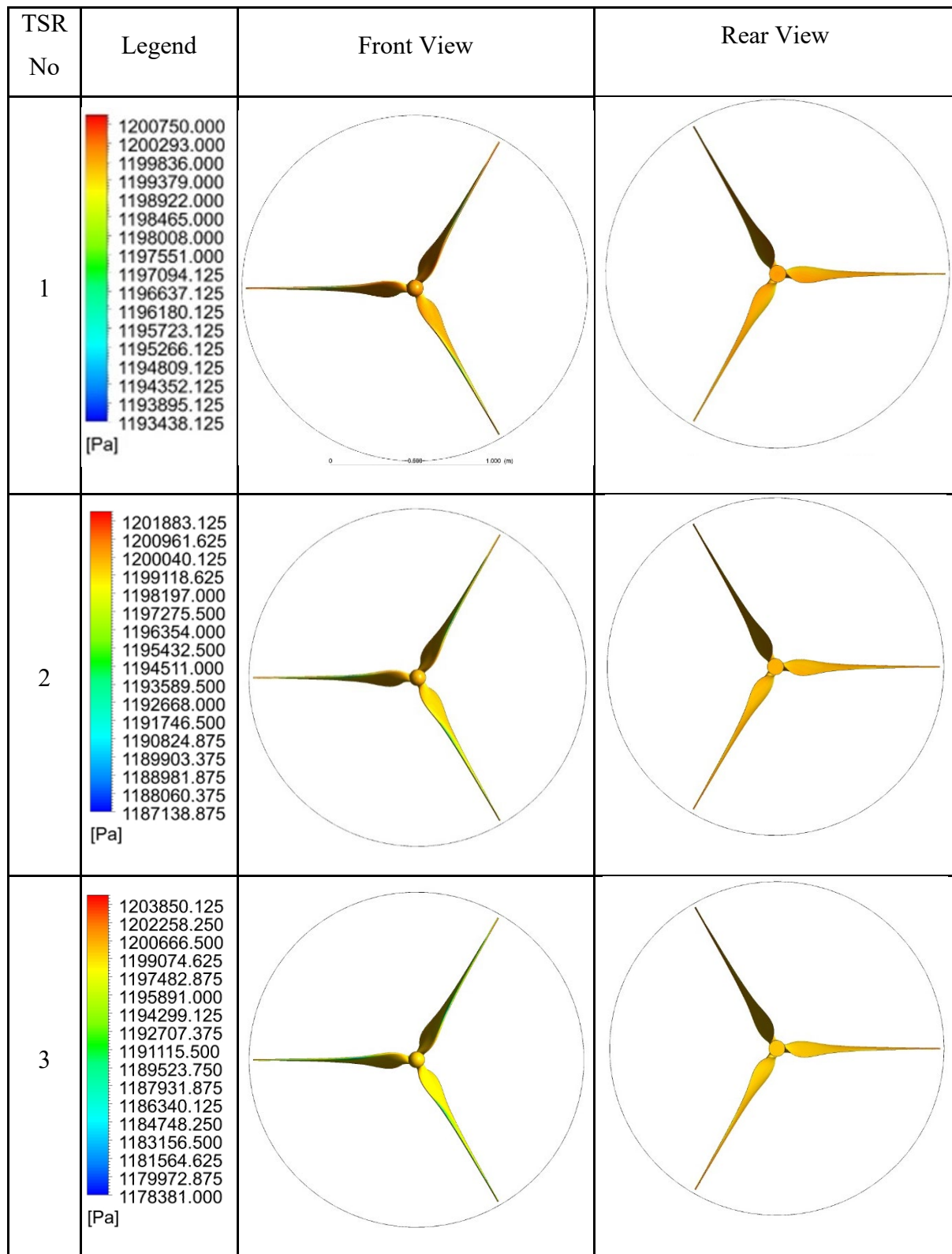
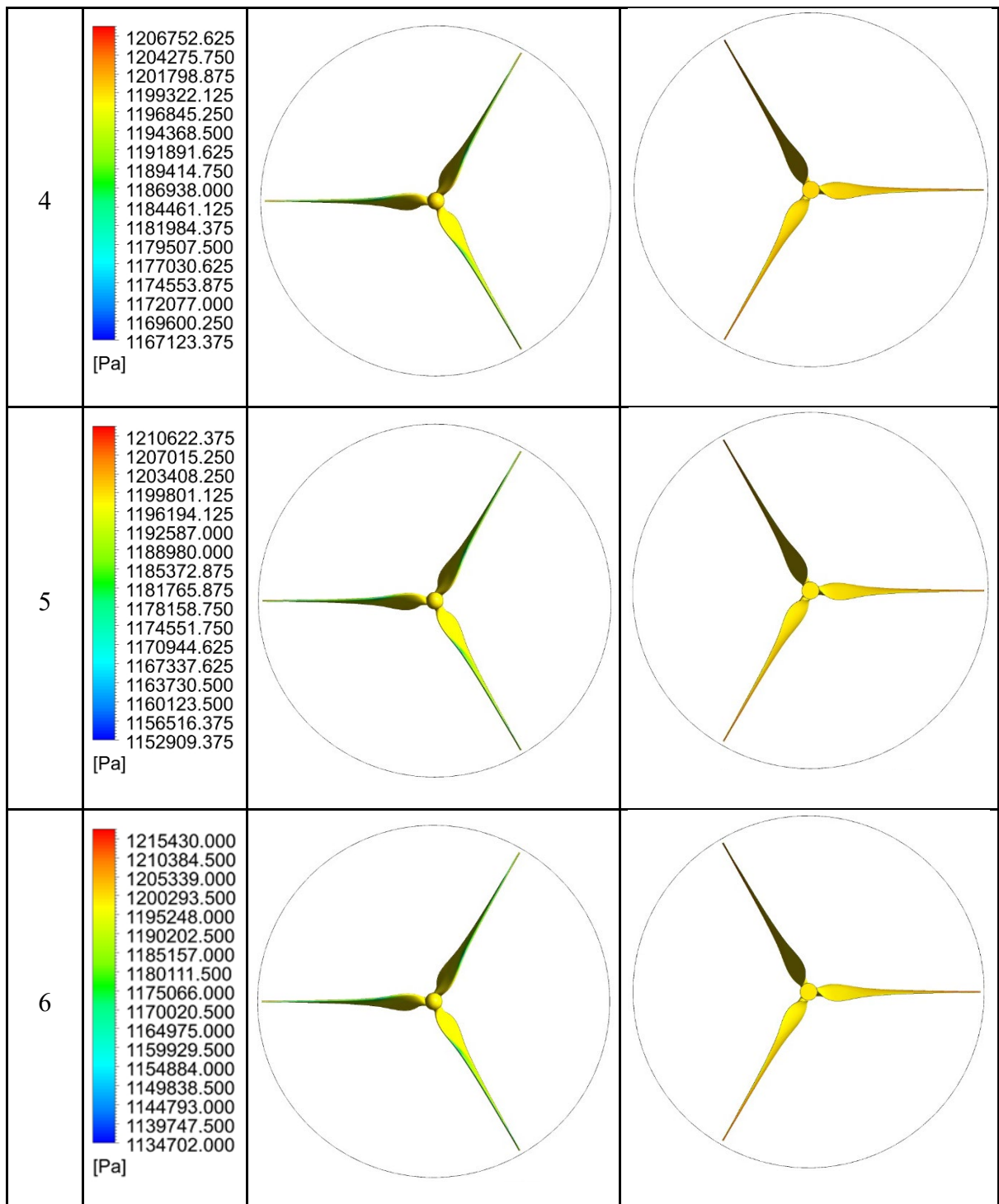


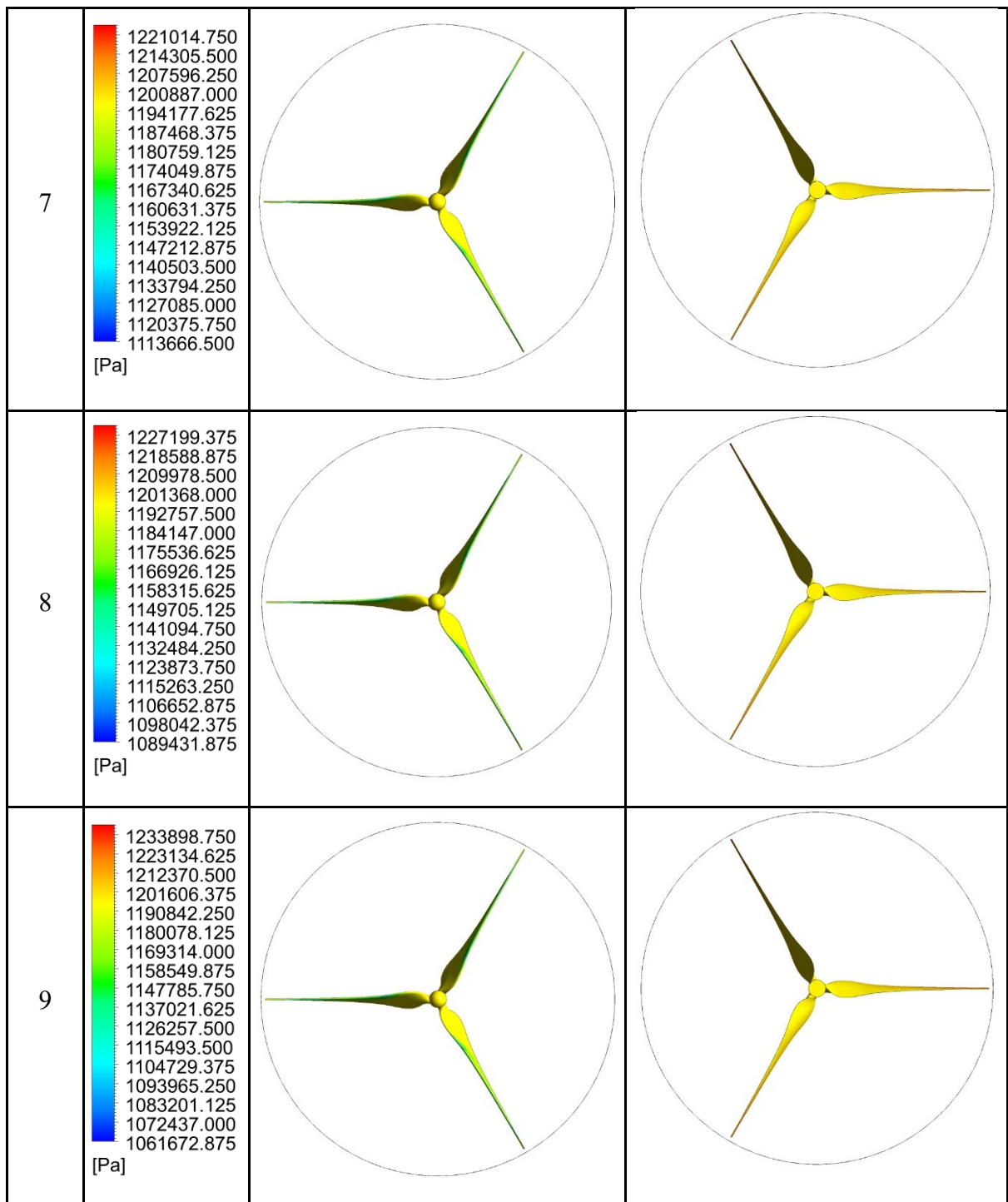
Fig 5.9: Residual Plot (Momentum)

After these plots from flow analysis simulation, the computational diagrams for Pressure Contours, Velocity Contours, Streamlines, Turbulence eddy frequencies contours, Turbulent Kinetic Energy, Eddy viscosity Contours, and finally velocity vectors for every tip speed ratio are produced.

As the surface area increases, the pressure of fluid acting on the blade also increases.  
 The pressure contours for different tip speed ratios are shown below.







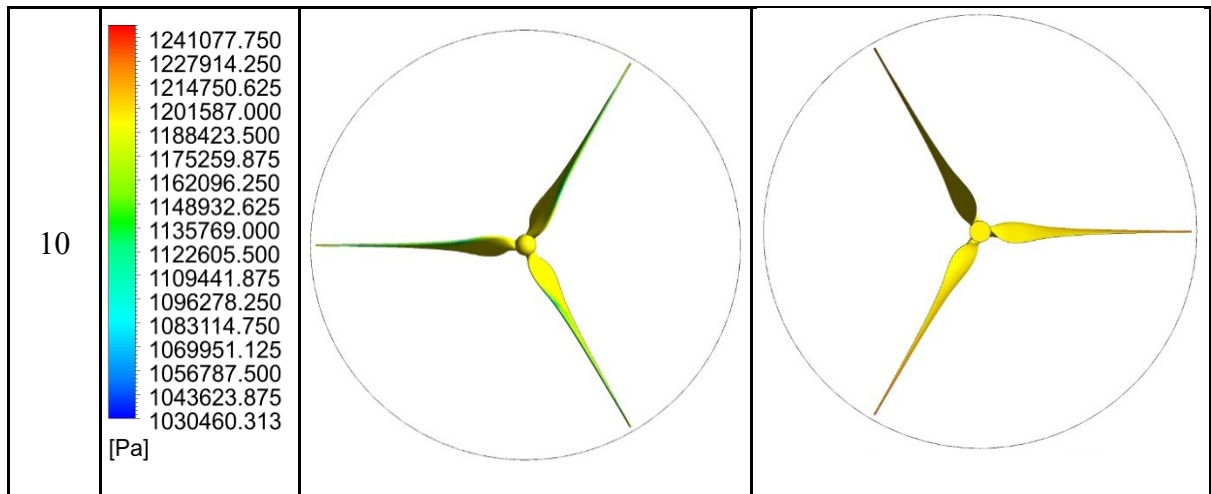
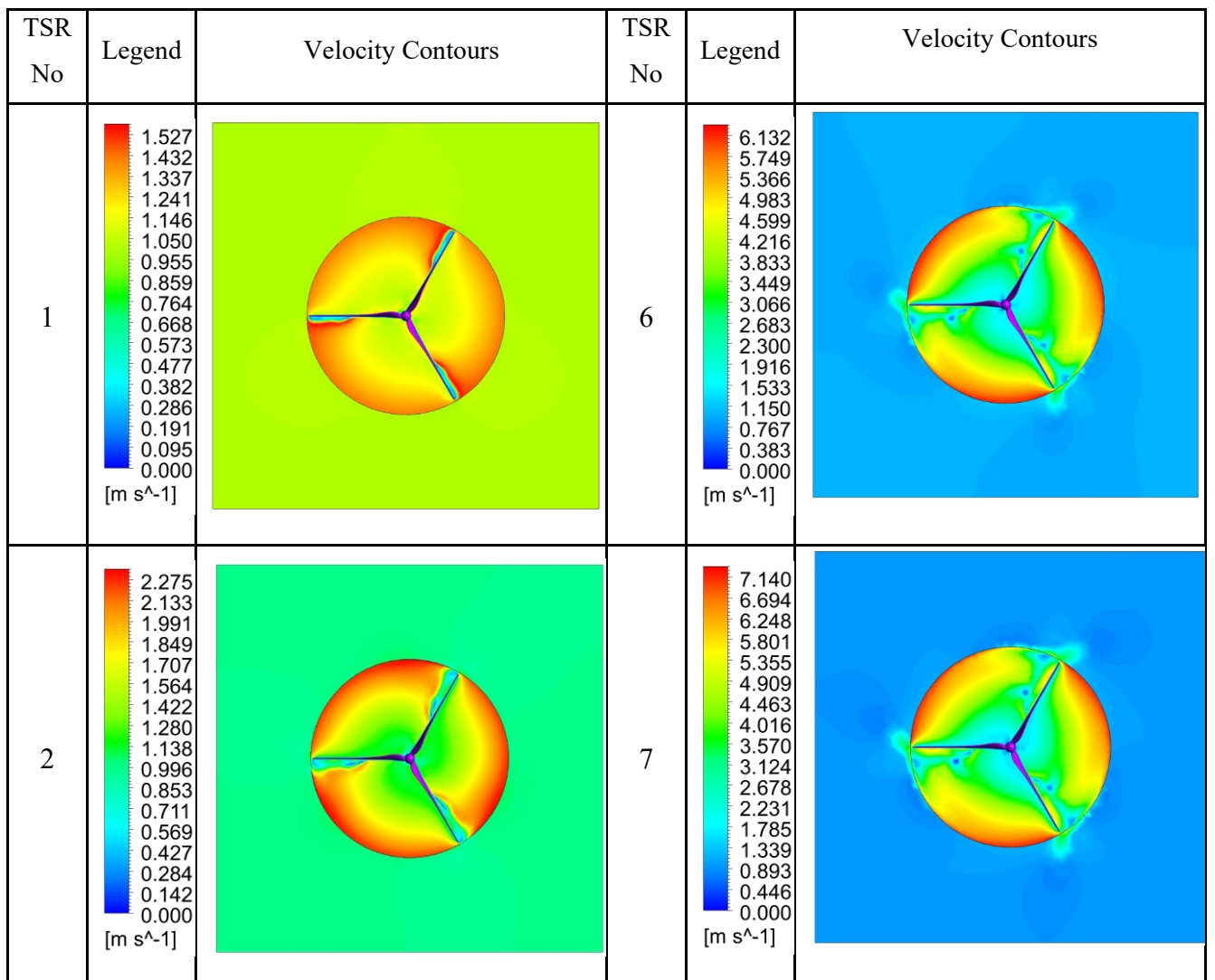


Fig 5.10: Pressure Contours

As the surface area increases, the obstruction of fluid will be more; then, there will be a decrease in the fluid velocity. From the below figure 5.11, it can be inferred that the velocity is increasing near the tip and significantly less near the hub.



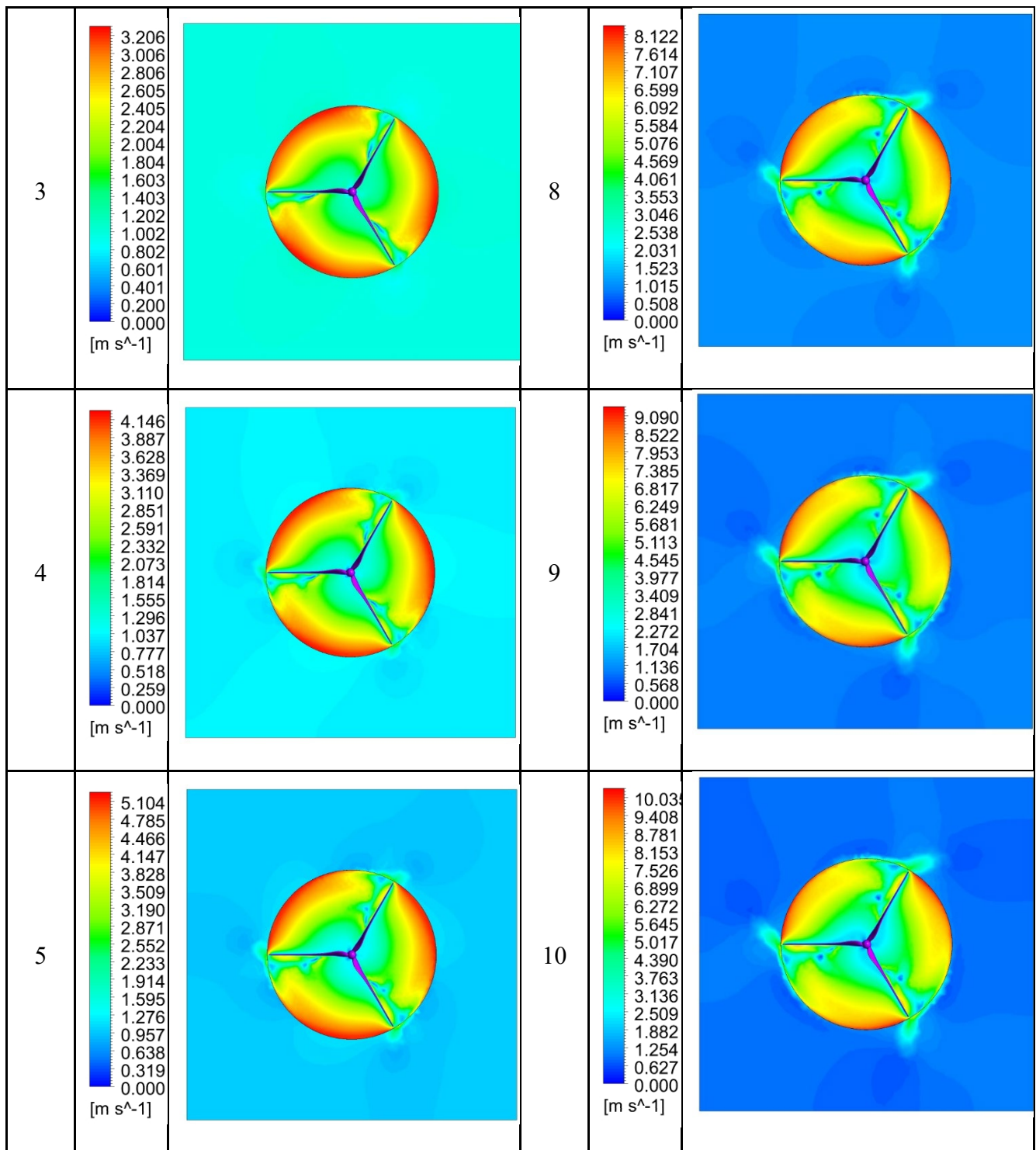
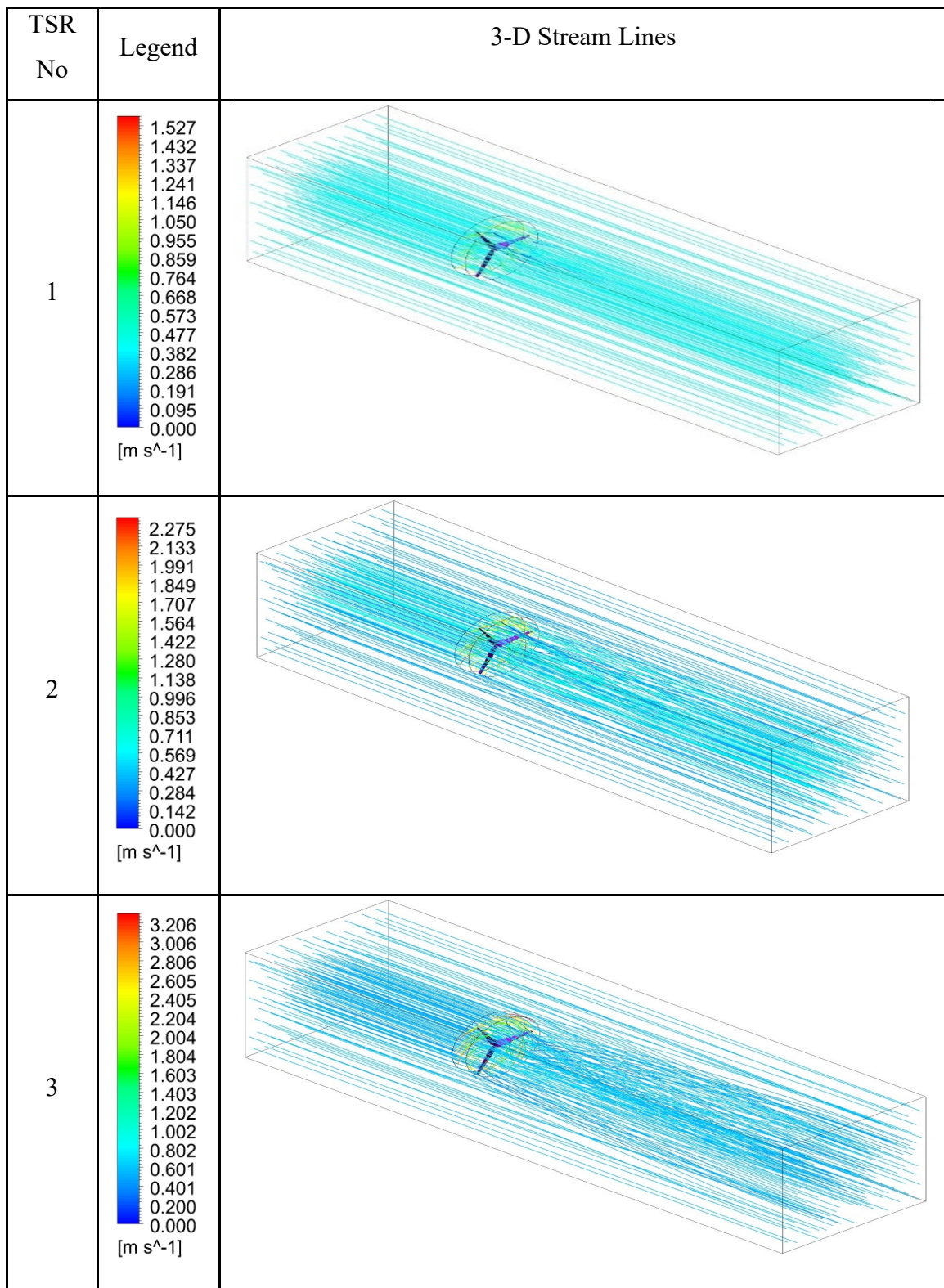
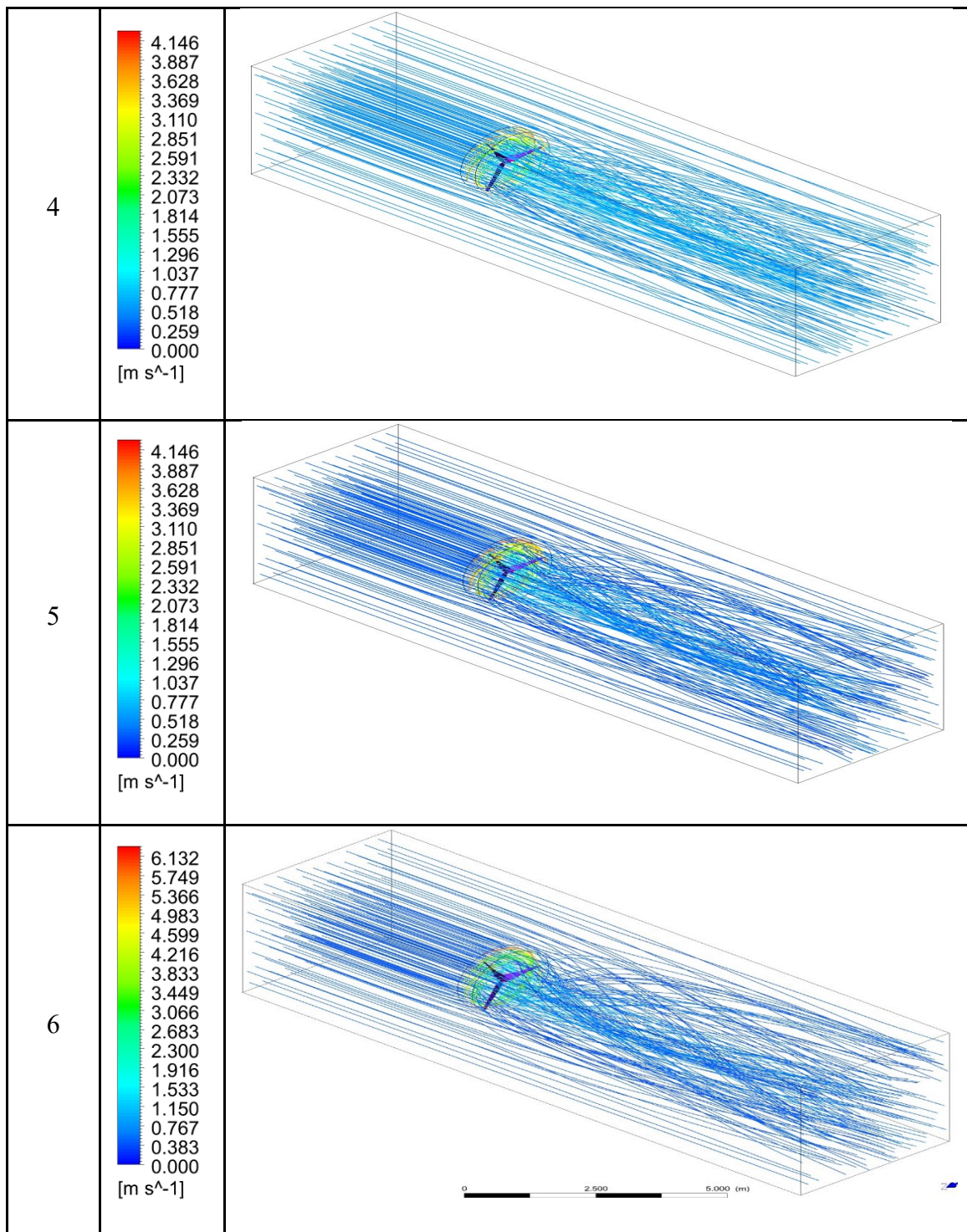
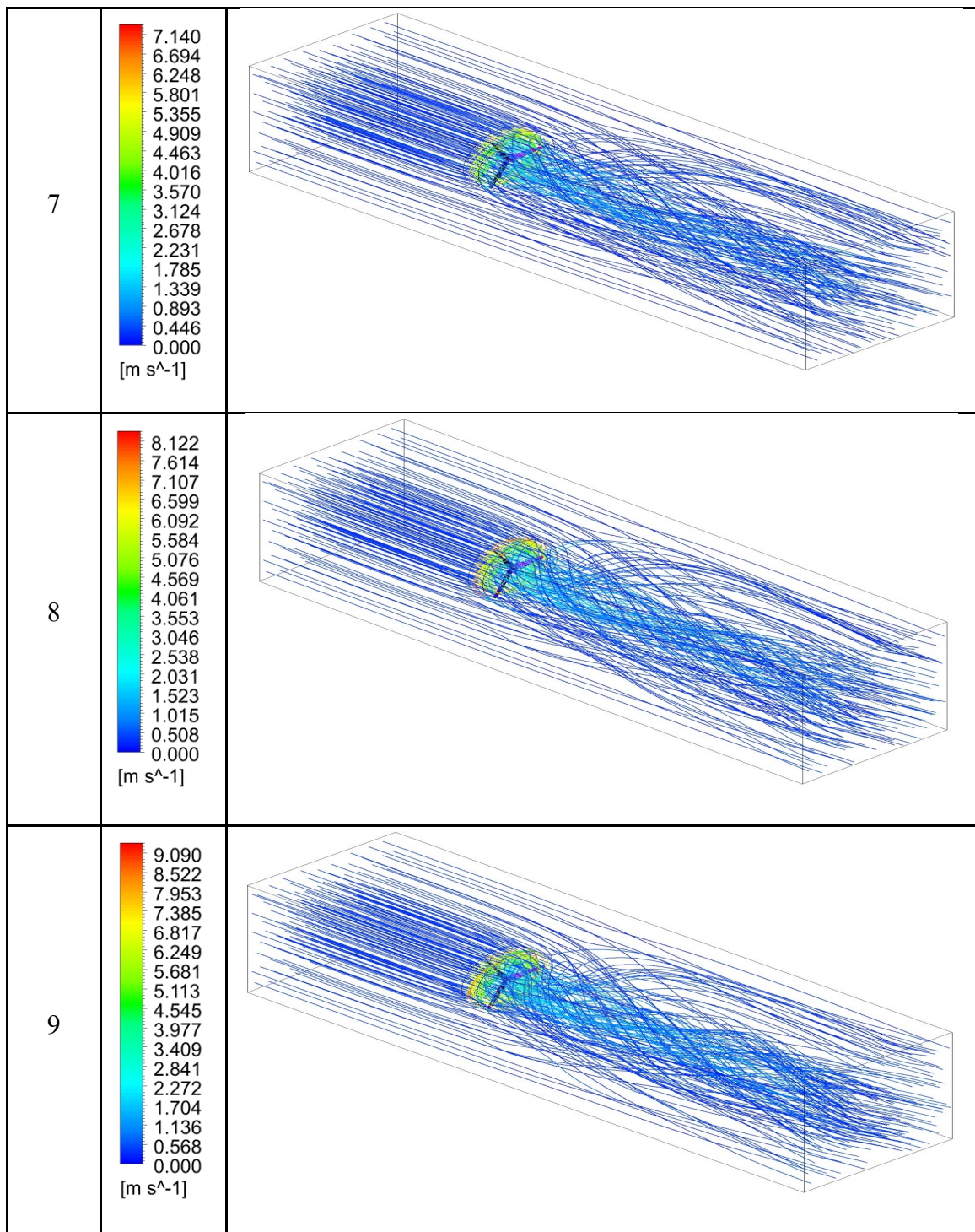


Fig 5.11: Velocity Contours

From below Fig 5.12 of 3-D streamlines, it gives a basic demonstration of fluid flow around the tidal turbine.







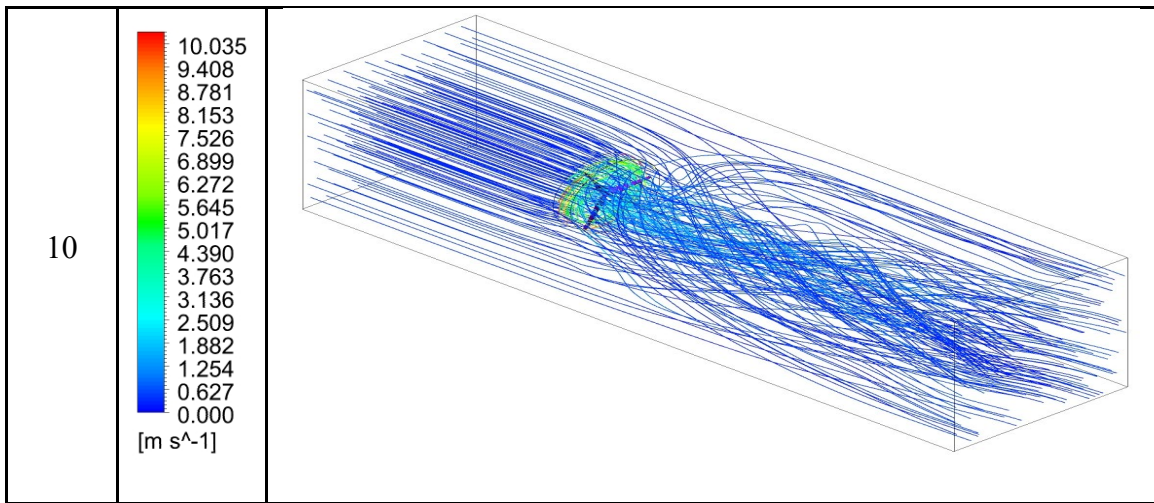
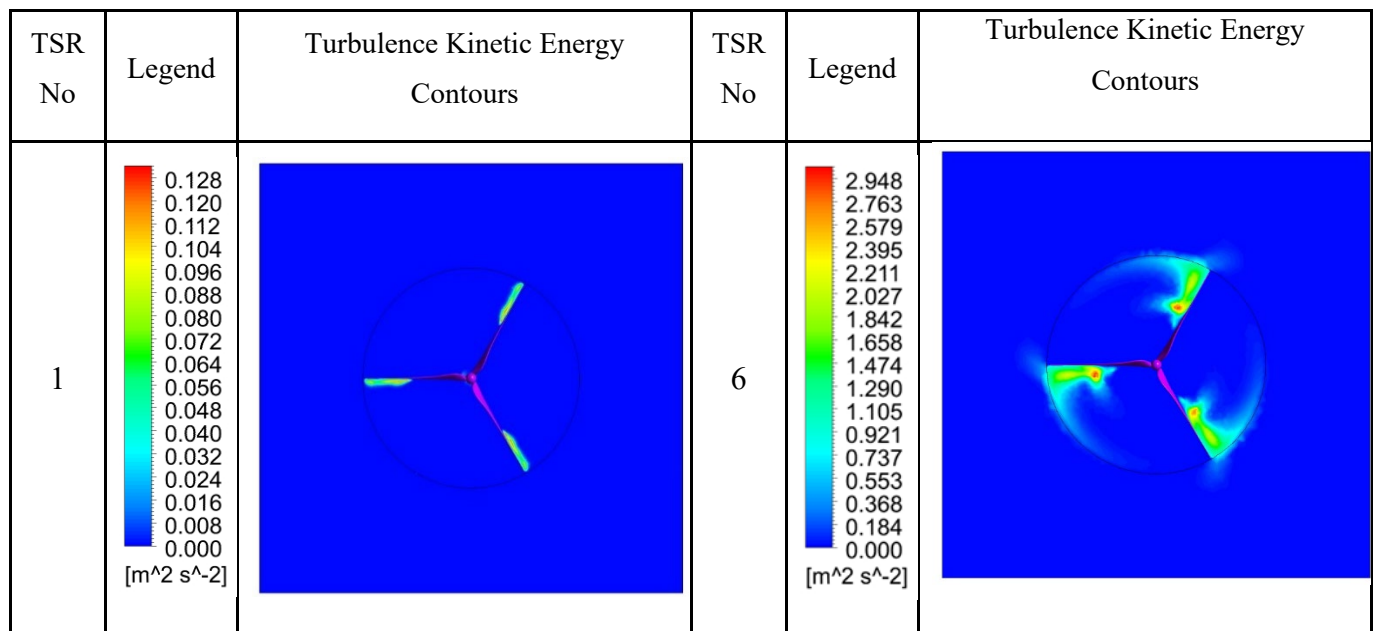
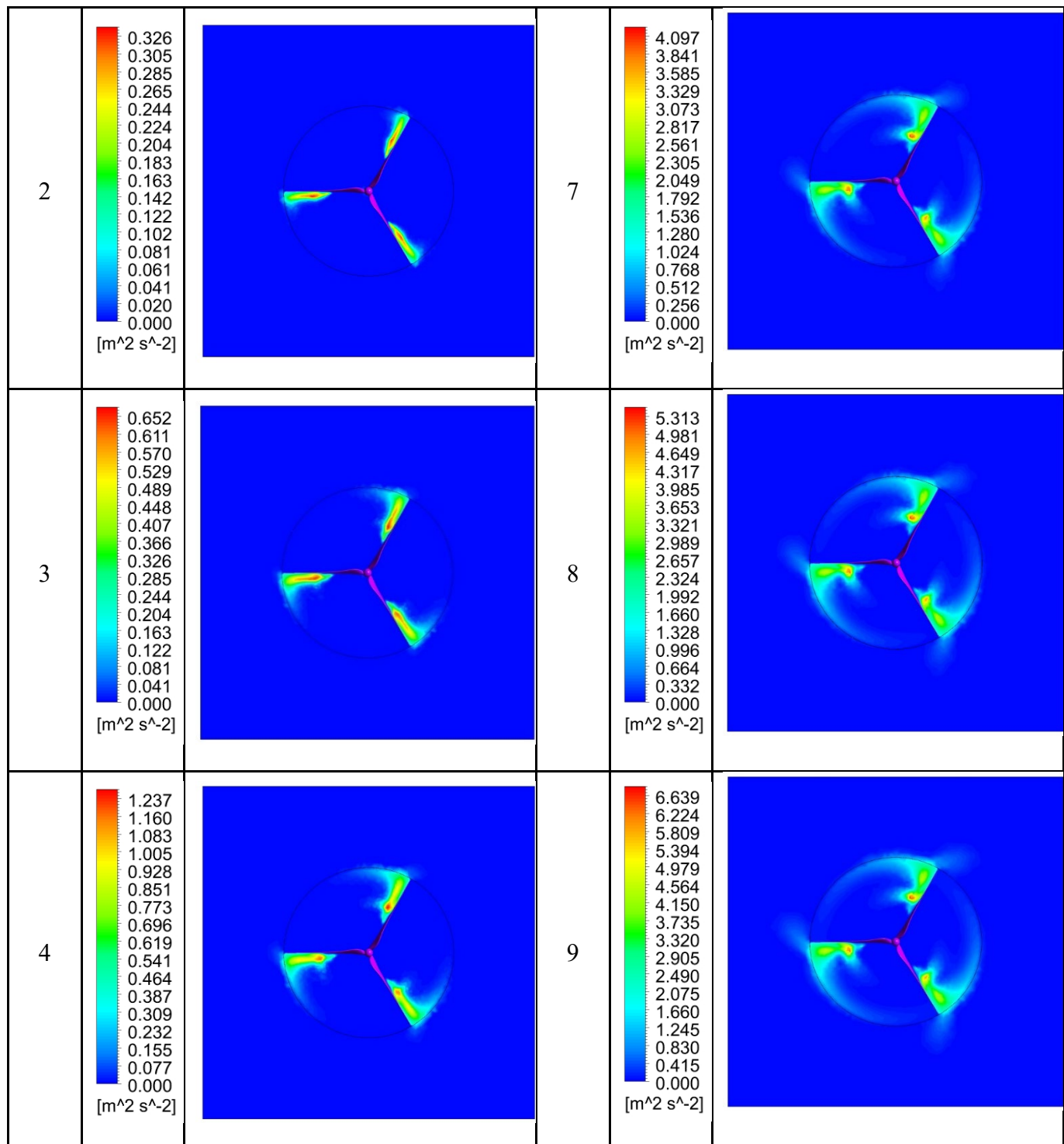


Fig 5.12: 3-D Stream Lines

Turbulent Kinetic Energy is the kinetic energy available in the turbulence behaviour of the fluid. The turbulent kinetic energy is more near the tip which will help in the rotation of the blade for which there is more energy extraction.





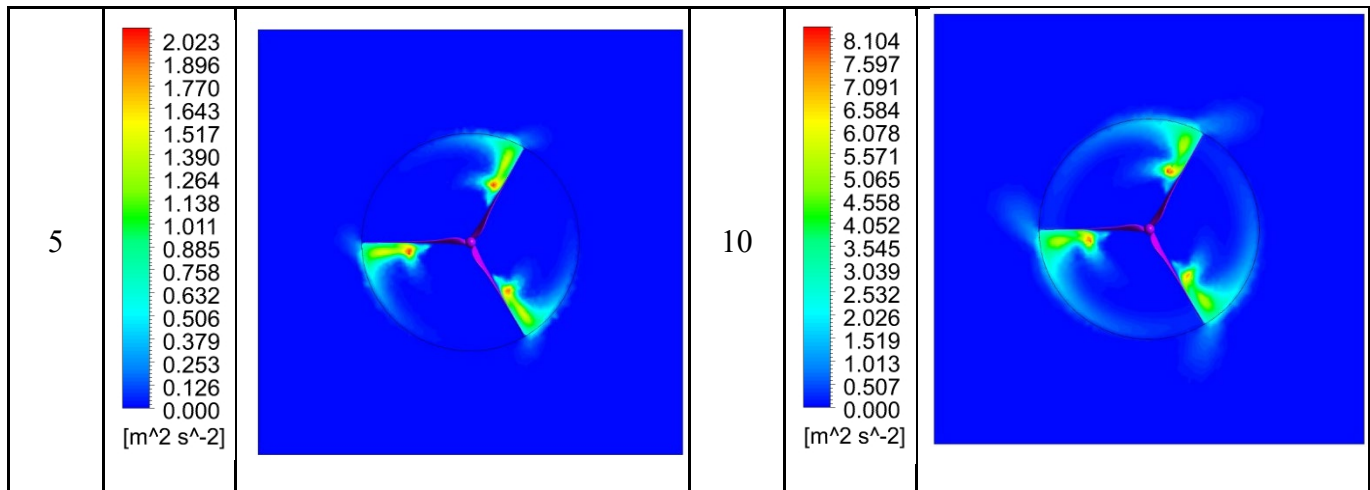
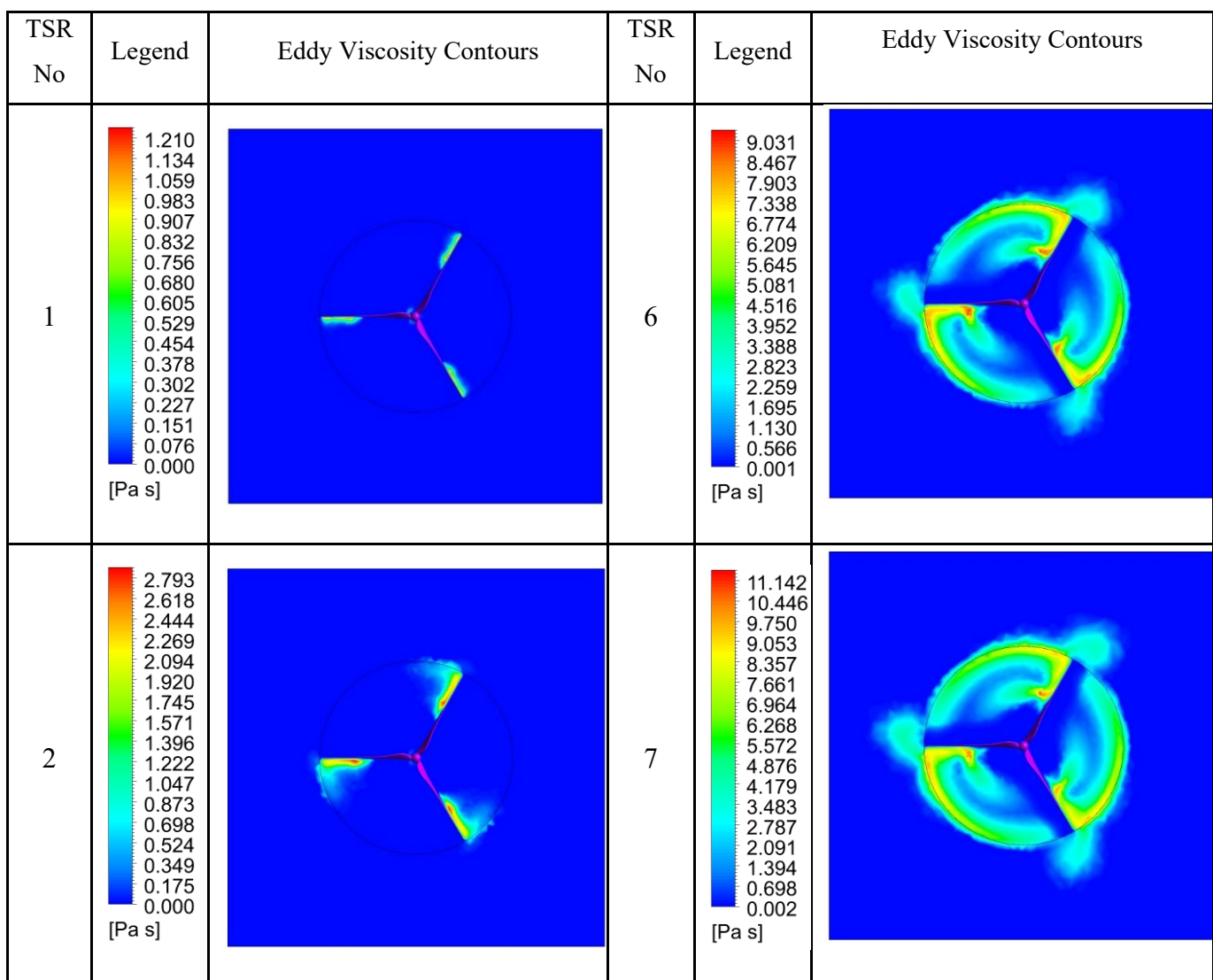


Fig 5.13: Turbulence Kinetic Energy Contours

Eddy viscosity is the resistance between the eddies in the fluid as the eddy viscosity increases, the velocity of seawater increases. Near the tip of the blades, there is more eddy viscosity. So, there is more velocity at tips.



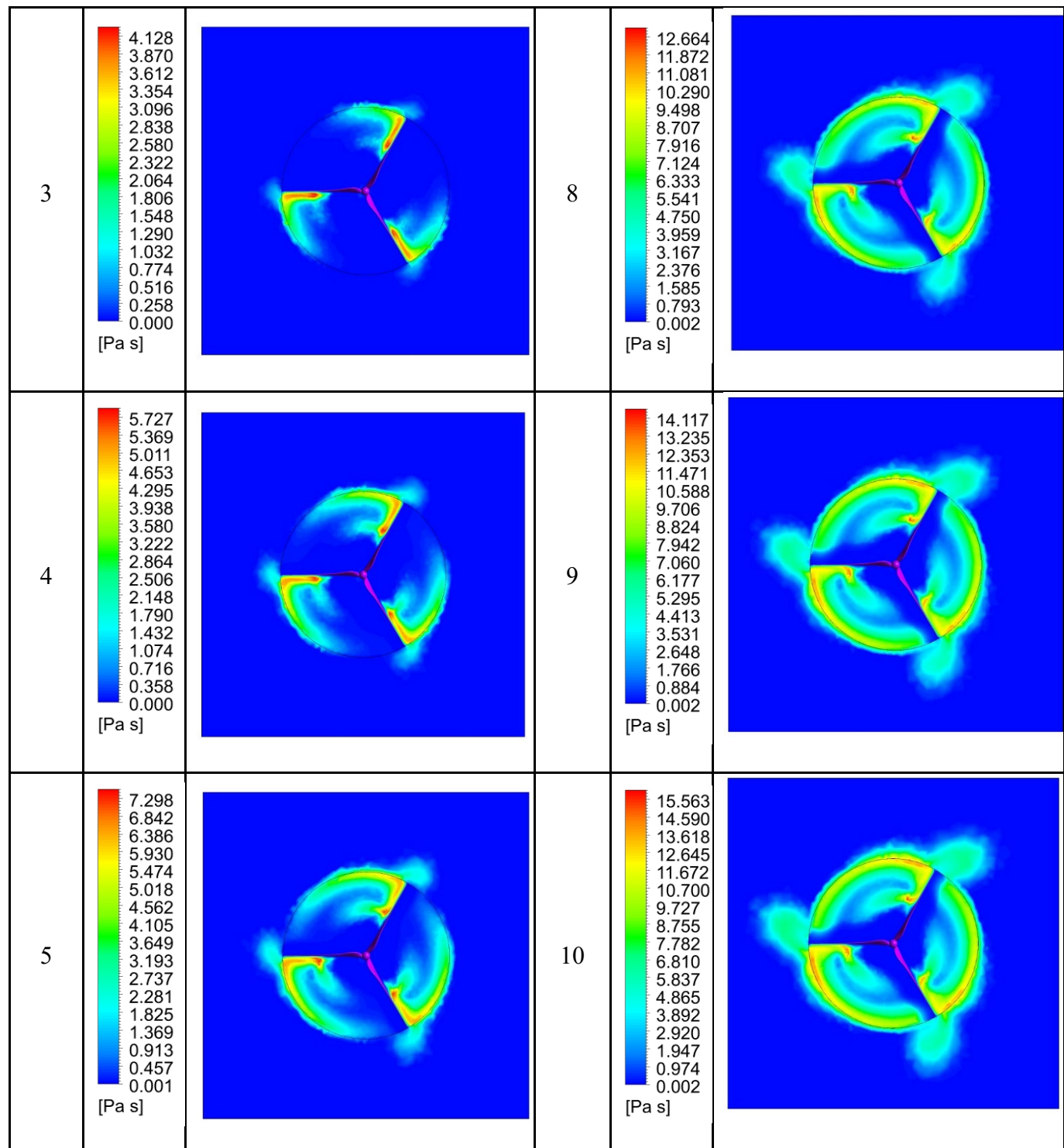
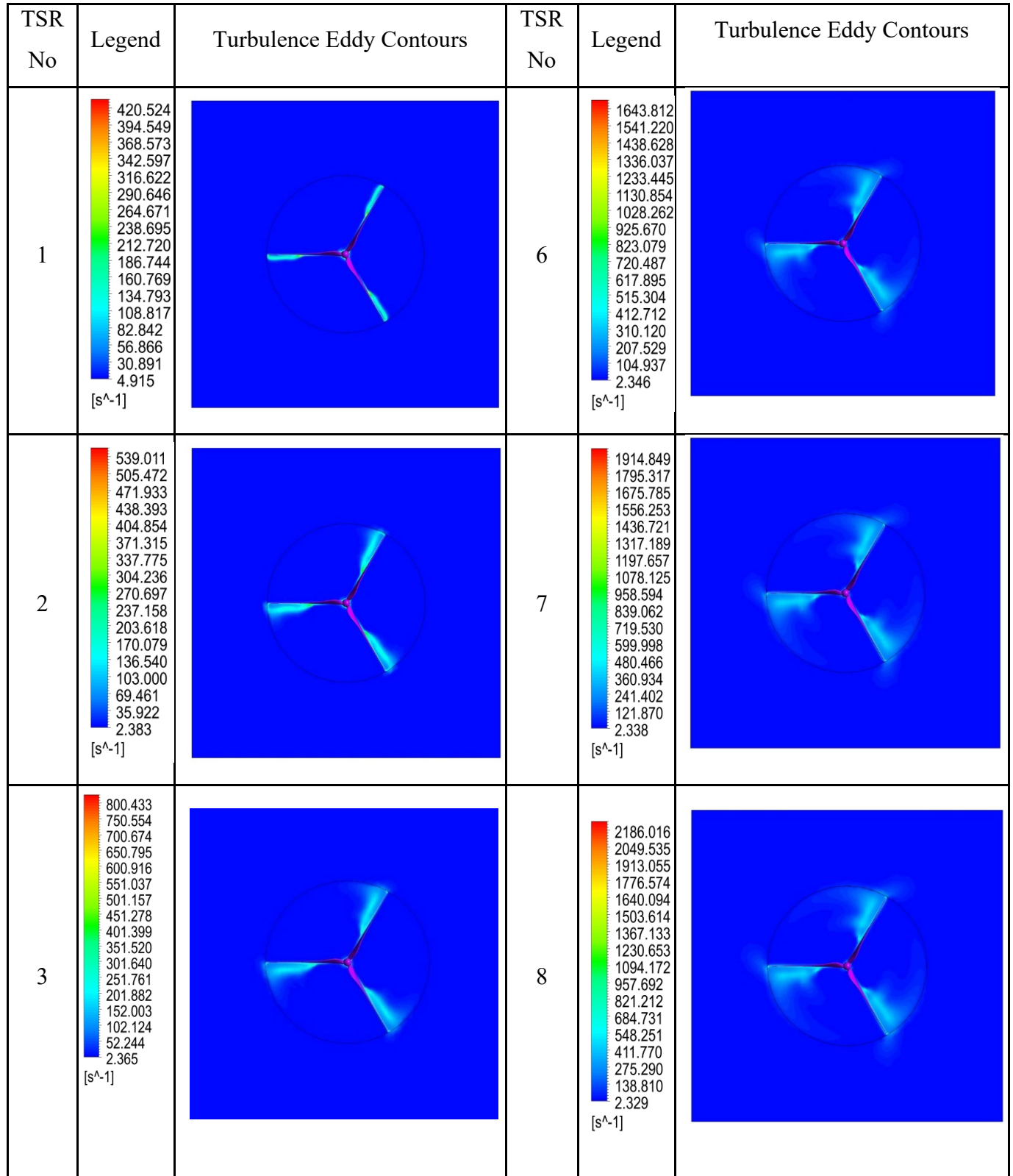


Fig 5.14: Eddy Viscosity Contours

Turbulent eddy frequency is the time scale of the turbulence eddy rotation. As it increases, these will account for more rotation of blades. The Turbulent eddy frequency Contours are shown below.



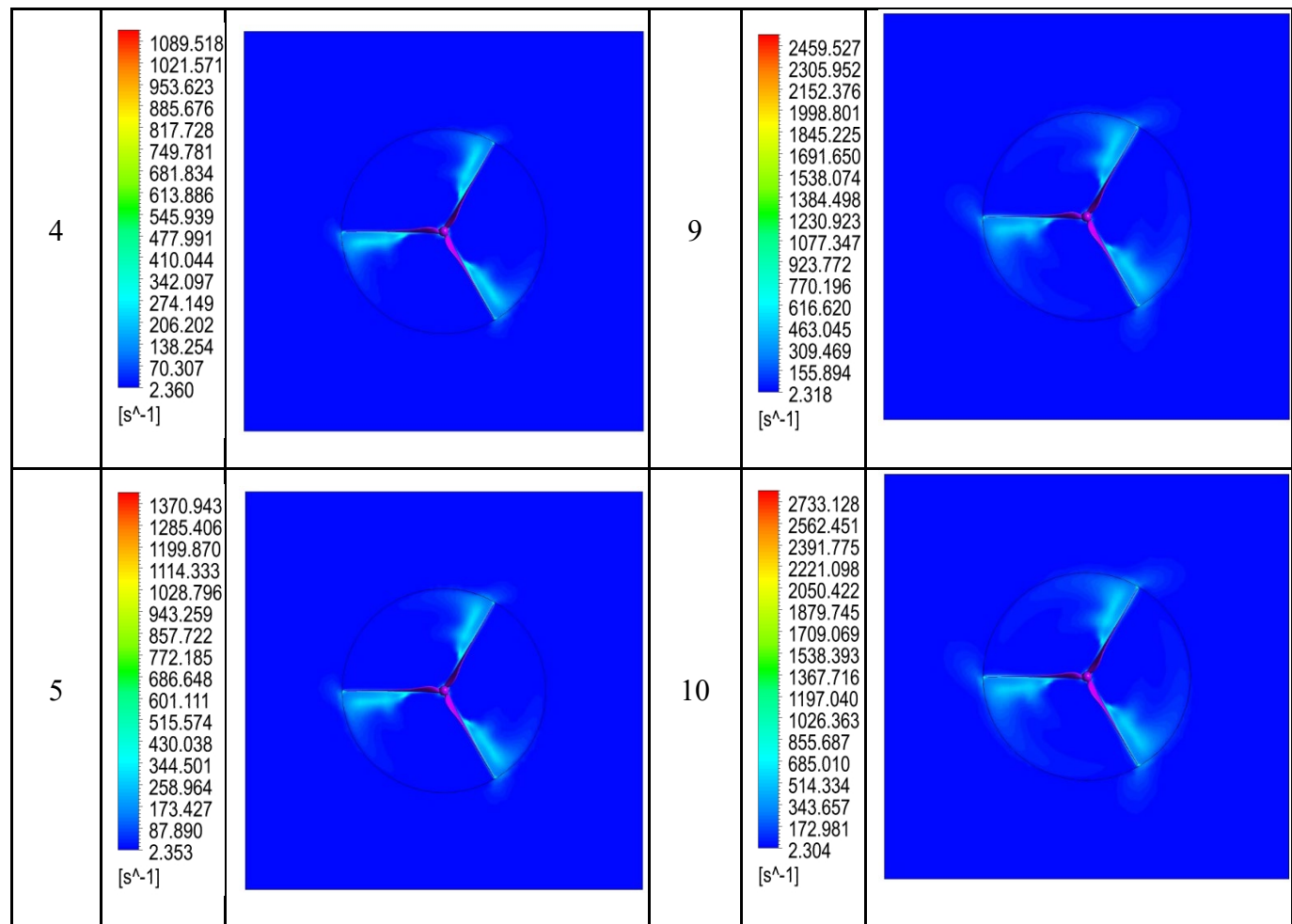
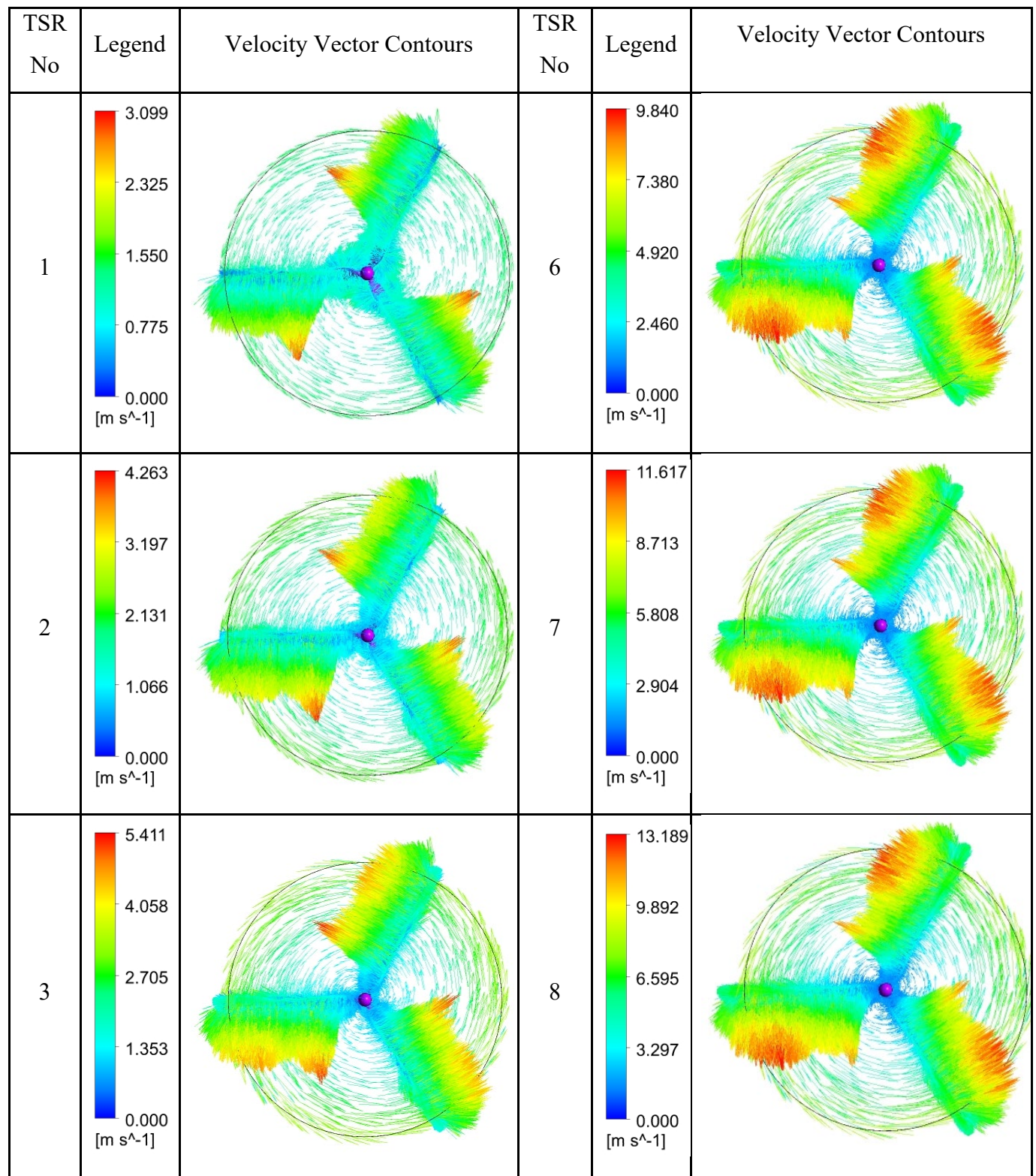


Fig 5.15: Turbulence Eddy Contours

The velocity vector gives us the magnitude of velocity and direction of a fluid particle. From the below contour results, how the fluid particles are directed around the rotor region is shown.



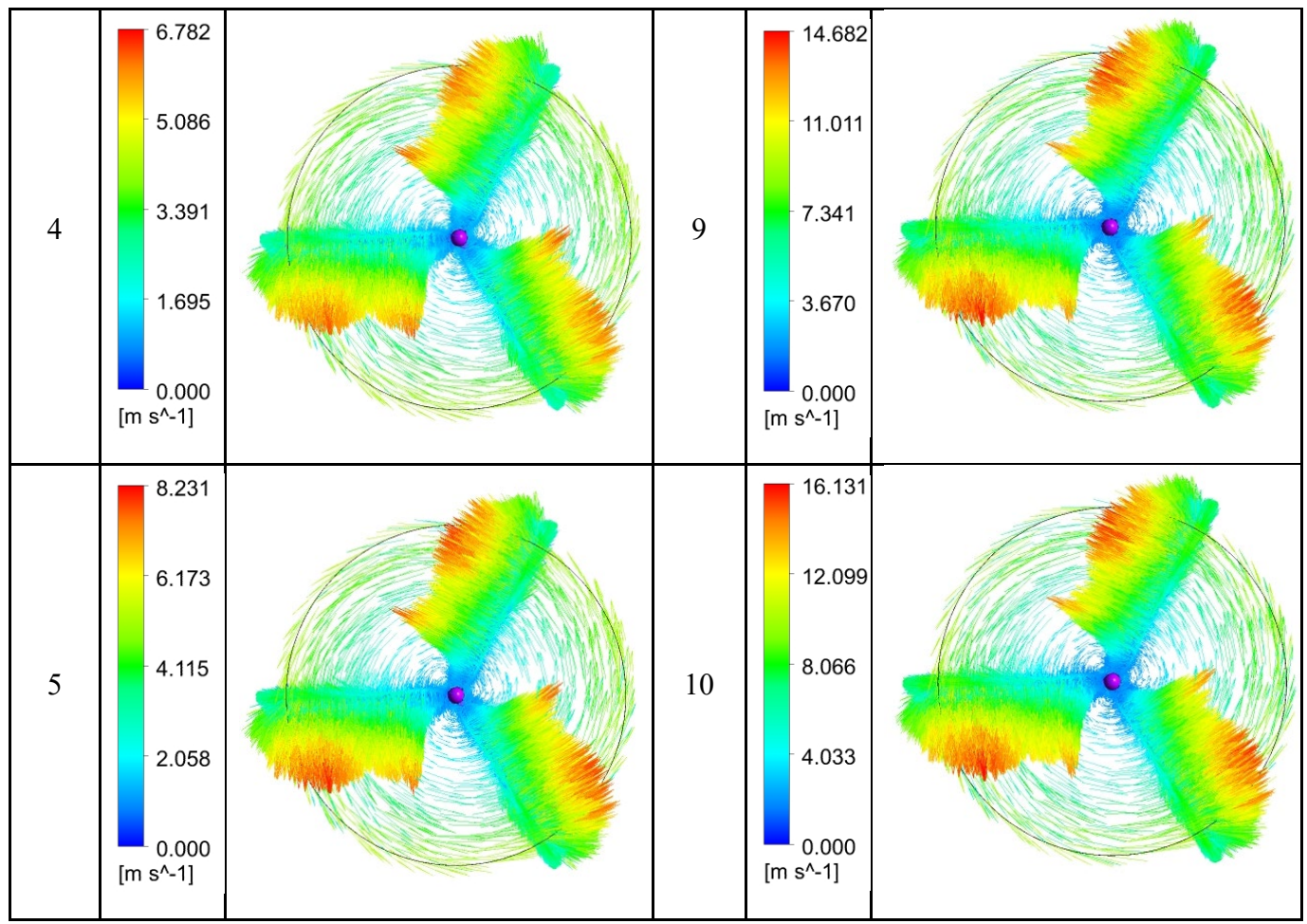


Fig 5.16: Velocity Vector Contours

From the TSR v/s Torque graph, when TSR increases, the torque also increases until it reaches the maximum at TSR5. After this, the torque will gradually decrease due to less speed at the hub than at the tip.

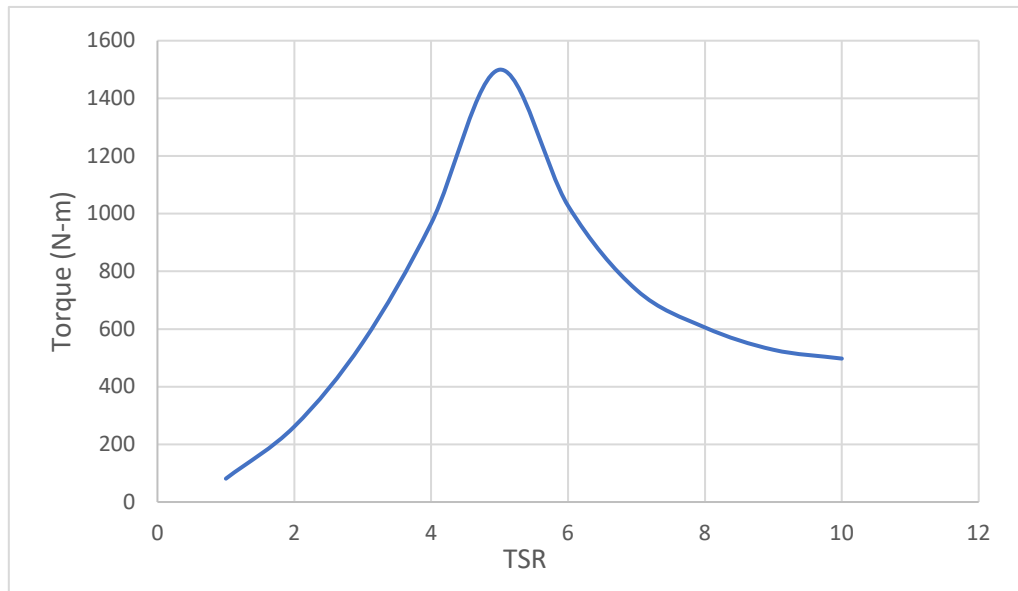


Fig 5.17: TSR v/s Torque (N-m)

From the TSR v/s Thrust force graph, when TSR increases, the thrust force also increases, but no thrust is generated, and a linear decrease will be there after reaching maximum thrust force. This is because lift forces acting on the blade will decrease since tidal turbine blades are drag-based turbines.

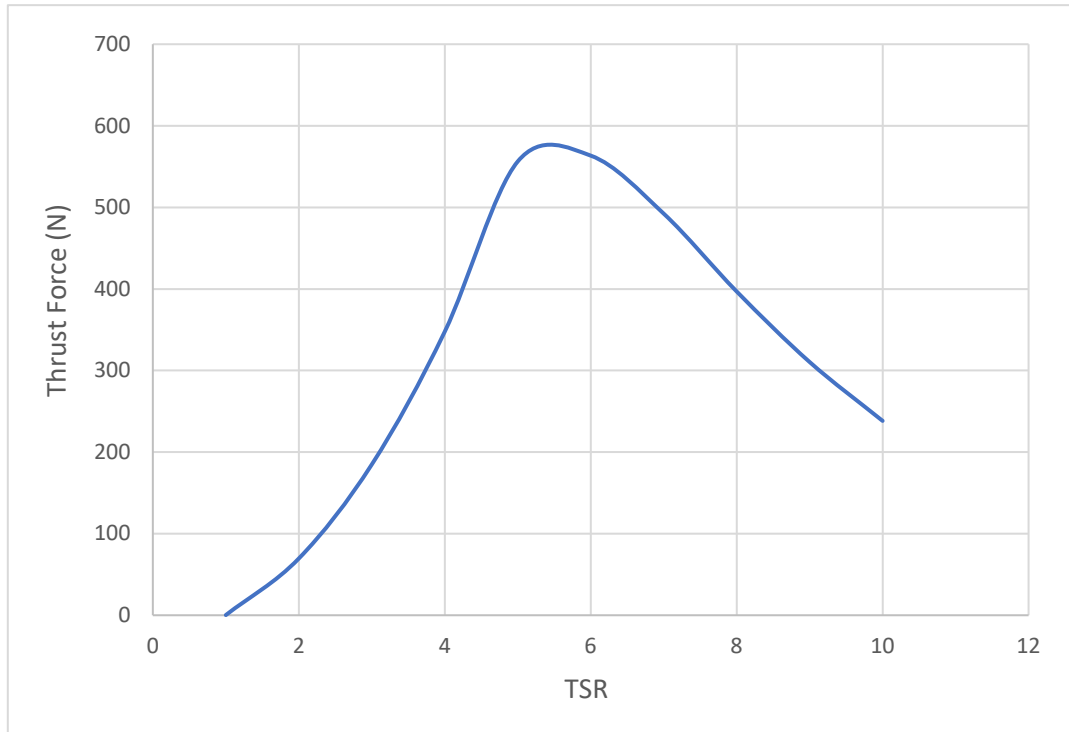


Fig 5.19: TSR v/s Thrust Force (N)

## **CHAPTER-6**

### **CONCLUSION**

The following results were drawn from this study's shape modelling of a tidal current power turbine based on turbine design theory and 3-D flow analysis using CFD. A horizontal axis tidal current power turbine was designed with a diameter of 2 m using NACA 4412 airfoil by considering tip loss based on turbine design theory, including blade element theory. This was embodied by using SOLIDWORKS, a 3D modelling program. Using ANSYS CFX V11 SP1, a commercial code, and conducting 3-d flow analysis on a 3D model, a performance curve and torque curve were drawn. At design flow 1.0 m/s, the maximum output coefficient was about 0.51 at a tip speed ratio of 5, and maximum torque was about 1499.45 N-m.

The effect of flow phenomena (pressure, direction, streamline distribution) around a turbine on the tip speed ratio was studied using a Post-processor to analyse the flow around the blade. As the tip speed ratio increases, negative pressure acting on the suction side increases, and at a more than optimal tip speed ratio, the output decreases because negative pressure occurs on the pressure side. Also, at a less-than-optimal tip speed ratio, output decreases due to turbulence on the suction side, and over the optimal tip speed ratio, the turbulence of the trailing edge reduces the output, and the significantly generated wake affects the flow of fluid.

Finally, we want to conclude that the model has almost negligible deformation from the Static Structural Analysis results. Mainly the model falls below the tensile yield strength, which is a good sign for the blade. The system rotation doesn't fall under the range of frequencies, and resonance is not in the frequency range from the model analysis. From the CFX flow analysis results, we have got the maximum torque and Thrust force at optimum tip speed ratio (TSR 5).

## **REFERENCES:**

### **Journals Papers:**

- [1] Chul Hee Jo, Jin Young Yimb, Kang Hee Leeb and Yu Ho Rhob. Performance of Horizontal Axis Tidal Current Turbine. *Renewable Energy*, 2011.
- [2] D. M. Grogan, S.B. Leen, C.R. Kennedy and C.M. Ó Brádaigh. Design of Composite Tidal Turbine Blades. *Renewable Energy*, 2013.
- [3] Alex E. Ockfen and Konstantin I. Matveev. Aerodynamic Characteristics of NACA 4412 Airfoil Section with Flap in Extreme Ground Effect. *International Journal of Naval Architecture and Ocean Engineering*, 2009.
- [4] Andreas Uihlein and Davide Magagna. Wave and Tidal Current Energy – A Review of The Current State of Research Beyond Technology. *Renewable and Sustainable Energy Reviews*, 2015.
- [5] Luthra, Sunil Kumar, Sanjay, Garg Dixit, and Haleem Abid. Barriers to Renewable / Sustainable Energy Technologies Adoption: Indian Perspective. *Renewable and Sustainable Energy Reviews*, 2014.
- [6] Kemp, P.H., and Simons R.R. The Interaction Between Waves and A Turbulent Current: Waves Propagating with The Current. *Fluid Mechanics*. 1982.
- [7] Sanil Kumar V., Dora G. Udhaba, Philip C., Pednekar P. and Singh Jai. Nearshore Currents along the Karnataka Coast, West Coast of India. *The International Journal of Ocean and Climate Systems*, 2012.
- [8] Chul Hee Jo and Su Jin Hwang. Review on Tidal Energy Technology on Research Subjects. *Chinese Ocean Engineering Society and Springer*, 2019.
- [9] Funke, S.W., Farrell, P.E. and Piggott, M.D. Tidal Turbine Array Optimisation Using the Adjoint Approach, *Renewable Energy*, 2014.
- [10] Sanjay V., Jain Rajesh and Patel N. Investigations on Pump Running in Turbine Mode: A Review of The State-Of-The-Art. *Institute of Technology, Nirma University*, 2013.
- [11] Couch S. J. And Bryden I. G. Tidal Current Energy Extraction: Hydrodynamic Resource Characteristics, *Proc. Imeche Vol. 220 Part M: J. Engineering for The Maritime Environment*, 2006.
- [12] Bae, Y.H., Kim, K.O. and Choi, B.H. Lake Sihwa Tidal Power Plant Project, *Ocean Engineering*, 2010.
- [13] Ko, D.H., Chung, J., Lee, K.S., Park, J.S. and Yi, J.H. Current Policy and Technology for Tidal Current Energy in Korea, *Energies*, 2019.

- [14] Brito E Melo A and Villate JL. Annual report 2013. Implementing Agreement on Ocean Energy Systems, 2013.
- [15] Bryden I. G. And Scott J. C. How Much Energy Can Be Extracted from Moving Water with A Free Surface: A Question of Importance in The Field of Tidal Current Energy? Journal of Renewable Energy, 2007.
- [16] Batten, W.M.J., Bahaj A.S., Molland A.F. and Chaplin, J.R. Experimentally Validated Numerical Method for The Hydrodynamic Design of Horizontal Axis Tidal Turbines, Ocean Eng. 2007.

**Books:**

- [1] D. M. Somers. The S814 and S815 Airfoil. National Renewable Energy Laboratory, 2004.
- [2] Peter J. Tavner. Wave and Tidal Generation Devices. British Library Cataloguing in Publication Data, 2017.

**Conference Proceedings**

- [1] Vikas M., Subba Rao and Jaya Kumar Seelam. Tidal Energy: A Review. Proceedings of International Conference on Hydraulics, Water Resources and Coastal Engineering, 2016.
- [2] Garbuglia E, Rosa A D, Berti D. Exploitation of marine current energy. Offshore Technology Conference, 1993.
- [3] Encarnacion, J.I. Johnstone, C. Preliminary Design of a Horizontal Axis Tidal Turbine for Low-Speed Tidal Flow. In Proceedings of the 4th Asian Wave and Tidal Energy Conference, 2018.
- [4] Walsum W. Offshore Engineering for Tidal Power. Proceedings of The Ninth International Offshore and Polar Engineering Conference, 1999.
- [5] Paish O. and Fraenkel P. Tidal Stream Energy Zero-Head Hydropower. International Conference on Hydropower into The Next Century, 1995.
- [6] Shiono M. Experiments on The Characteristics of Darrius Turbine for The Tidal Power Generation. Proceedings of The Ninth International Offshore and Polar Engineering Conference, 1999.
- [7] Jo CH, Lee CH, Rho YH and Yim J.Y. Floating Tidal Current Power Application in Cooling Water Channel. The Korean Association of Ocean Science and Technology Societies Conference, 2008.